Journal of Hydropower and Civil Engineering

Volume No. 8

Issue No. 1

January - April 2024

ENRICHED PUBLICATIONS PVT. LTD

S-9, IInd FLOOR, MLU POCKET,
MANISH ABHINAV PLAZA-II, ABOVE FEDERAL BANK,
PLOT NO-5, SECTOR-5, DWARKA, NEW DELHI, INDIA-110075,
PHONE: - + (91)-(11)-47026006

Journal of Hydropower and Civil Engineering

Aims and Scope

Journal of Hydropower and Civil Engineering envisage to publishes best of reviews and researches within the broad field of civil engineering which include construction management, geotechnical engineering, transportation engineering, concrete technology, and very importantly the water engineering

Journal of Hydropower and Civil Engineering

Journal of Hydropower and Civil Engineering

(Volume No. 8, Issue No. 1, January - April 2024)

Contents

Sr. No.	Title / Authors Name	Pg. No.
1	Flume Study On Bridge Pier Scour Embedded Within Long Contraction For Clay-Sand Mixed Cohesive Sediment Bed – *Susanta Chaudhuri Koustuv Debnath and Mrinal K. Manik*	01 - 09
2	Multiple Inflow River Flood Routing Using ANN – *Bahnisikha Das, Ruhul Amin Mozumder, B S Sil*	10 - 18
3	Transient in Systems, Prentice-Hall, Englewood Cliffs. – *Prabhat Kumar, Pranab K. Mohapatra*	19 - 27
4	Prediction Of Training Wall Height For Convergent Stepped Spillway - A Model Study – *P. J. Wadhai, A. D. Ghare,N. V. Deshpande*	28 - 40
5	Determination Of Residual Energy For Flow Over Trapezoidal Labyrinth Weir – *Dr. Bhalchandra V. Khode*	41 - 48

Flume Study On Bridge Pier Scour Embedded Within Long Contraction For Clay-Sand Mixed Cohesive Sediment Bed

Susanta Chaudhuri[1] Koustuv Debnath[2] and Mrinal K. Manik[3]
[1]Department of Geological Sciences, Jadavpur University, Kolkata, 700032, India
[2] Fluid Mechanics and Hydraulics Laboratory, Department of Aerospace Engineering and
[3]Applied Mechanics, Indian Institute of Engineering Science and Technology, Shibpur, Howrah, 711103, India
Email; schaudhuri1997@gmail.com
Mobile No.: +91 9830991788

A B S T R A C T

Contractions of river width to construct bridges, barrages, weirs and cross-drainage works are common examples of channel contractions. The flow velocity in the contracted zone of the channel increases due to the reduction of flow area, and hence the bed shear stress induced by the flow increases considerably. In normal practice either abutments or guide walls are generally constructed at the bank of the river for erection of a bridge, which reduces the width of flow considerably. As a result of such constriction, the development of contraction scour, enlarged scour hole with increased equilibrium scour depth occurs at the base of the bridge piers embedded within the zone of contraction. A contraction generally termed 'long contraction' when the longitudinal length of contracted zone is greater than the transverse width of the flow. Till now no investigation has been reported on bridge pier scour embedded within long contraction for clay – sand mixed cohesive bed. In the present study an attempt has been made to study the bridge pier scour embedded in long contraction for the bed sediment prepared by a mixture of clay and fine sand with varying proportions with a specific range of antecedent moisture content. New empirical data on pier scour embedded within long contraction in clay-sand mixed cohesive sediment beds are reported. Results of 90 experimental runs on clay-sand mixed cohesive bed were studied to investigate the effect of varying clay fraction of the sediment bed, approach flow velocity, contraction ratio and different pier shapes, on maximum equilibrium scour depth for pier scour within long contraction.

Keywords: Flume Study; Pier Scour; Long Contraction; Cohesive Sediment

1. INTRODUCTION

Flow constriction, whether man-made or natural, occurs whenever there is a significant reduction of the width of a canal or river. The effect on the flow is an increase in the velocity and bed shear stress, which may cause local scour within the contracted reach. The problem is often idealized as a rectangular long contraction shown in the figure 1.a consisting of a channel with gradual reduction in width from b_1 to b_2, where b_1 = approach channel width and b_2 = opening width at the constriction and contraction ratio is being denoted by the symbol bc, where $bc = b_2/b_1$. According to Kumura (1966) and Raikar (2005), a contraction becomes long when $L/b_1 > 1$. A series of empirical equations on contraction have been proposed by Laursen (1960), Komura (1966), Gill (1981), Lim and Cheng (1998) and Briaud et al (2003).

In all the investigations, bed sediment used were non cohesive sand beds, except Briaud et al (2003), where bed sediment was made up of Kaolinte clay. It is also revealed from the literatures that till now no such investigation has been reported on pier scour embedded within long contraction for clay – sand mixed cohesive bed. In the present study an attempt has been made to study the pier scour within long contraction for the sediment bed made up of a mixture of clay and fine sand with varying proportions having a specific range of antecedent moisture content (W_c). In this work results of 90 experimental runs on clay-sand mixed cohesive bed were studied to investigate the effect of varying clay fraction (C), approach flow velocity (U), contraction ratio (b_c) and different pier shapes (square and circular) on maximum equilibrium scour depth (y_s) for bridge pier scour embedded within long contraction.

2. EXPERIMENTAL SETUP AND PROCEDURE

Experiments were conducted at the 18.3m long, 0.9m wide and 0.9m deep tilting flume (kept at constant slope = 0.001) located in the Fluid Mechanics and Hydraulics Laboratory, Indian Institute of Engineering Science and Technology, Shibpur, Howrah, India. The flow of the flume was contracted by using perspex made contraction models having uniform contraction zone (L) of 1 m length. Contraction models of two opening ratios (= $b_c = b_2/b_1$; where b_1 = approaching channel width; and b_2 = width of the contracted zone) of 0.77(b_1 = 90cm, b_2 = 40cm) and 0.44 (b_1 = 90cm, b_2 = 40cm) were used. Figure 1(a, b) depicts the schematic diagram of the experimental set up. A point gauge and a 16 MHz Micro ADV, mounted on instrument carriage were used to measure scour hole profiles and flow characteristics, respectively.

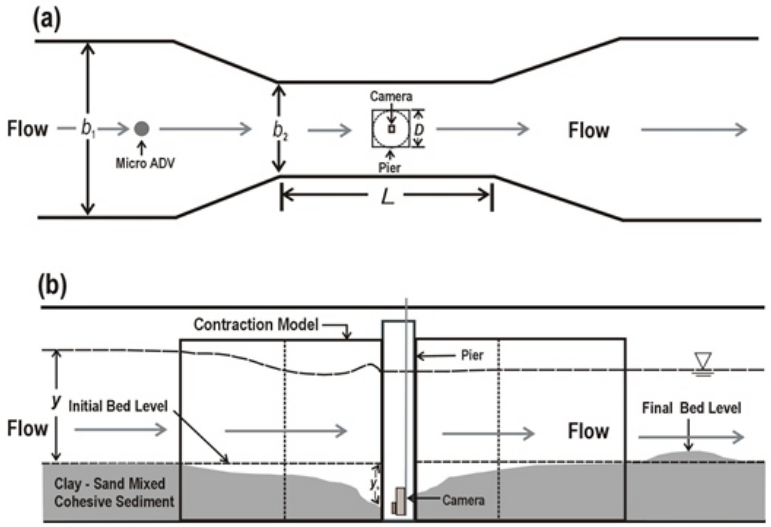

Figures 1(a-b) Schematic view of experimental set up (a) top view and (b) side view (not to scale)

The mean velocity profile could be approximated well by the log law (e.g., Nezu and Nakagawa 1993). Transparent circular and square cylinder made of Perspex (D = 12cm) were used for the experiments, where D is the transverse length of pier models. Vertical graduated tapes at 0° (front), 90° (left side), and 180° (behind), 270° (right side) were attached to the circular pier models. In addition, for the square pier model, additional tapes were attached at 45° (left side front corner) and 315° (right side front corner). A NB Pro-Logitech camera connected with computer and installed inside the pier model from a carriage unit (camera holder) with vertical and rotational degrees of freedom, was used for recording the final maximum equilibrium scour depth against the attached scales. Figures 2.a-b depicts the positions of attached scales within the pier models.

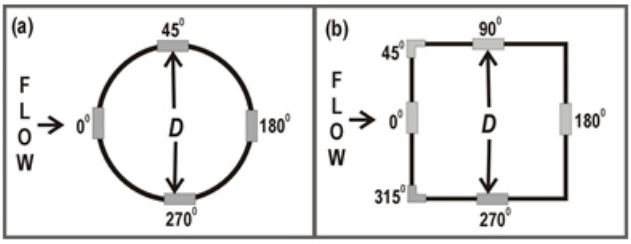

Figures 2(a-b) Schematic diagrams showing the positions of attached scales within the pier models

Ranges of experimental conditions and observed results are shown in Tables 1. Here experimental ranges and results for run no. 61 – 90 were taken from the previous experimental works of Denath and Chaudhuri (2012) for the purpose of comparison. These experimental runs (run no. 61 – 90) were conducted at normal un-contracted flow condition i.e. $b_c = 1.00$ (where $b_1 = 90$cm) with same background conditions of flow parameters and sediment characteristics. Experiments were conducted at three ranges of flow velocity for individual pier shape, b_c and sediment bed i.e. $U_1 = 49.25 – 53.91$ cm/s, $U_2 = 59.10 – 62.93$ cm/s and $U_3 = 69.79 – 72.78$ cm/s. Detailed procedure of experimentation can be found in Debnath and Chaudhuri (2010a, b).

Table 1 Ranges of experimental conditions and results

Run No.	b_c	Pier Shape	C	W_c	τ_s (N/cm²)	U (cm/s)	y_s (cm)	$\hat{y}_s$	y_s location Scale	T_e (hrs)	T_e (hrs)
1 - 15	0.44	Circular	0.35 - 1.00	0.299 - 0.327	0.740 - 1.400	50.40 - 71.33	14.70 - 26.10	1.23 - 2.18	270° for 12 runs 90° for 3 runs	57 - 72	67 - 82
16 - 30	0.44	Square	0.35 - 1.00	0.289 - 0.326	0.748 - 1.210	50.80 - 71.53	21.80 - 39.20	1.82 - 3.27	315° for 9 runs 45° for 6 runs	48 - 63	58 - 73

Run No.	b_c	Pier Shape	C	W_c	τ_s (N/cm²)	U (cm/s)	y_s (cm)	$\hat{y}_s$	y_s location Scale	T_e (hrs)	T_c (hrs)
31 - 45	0.77	Circular	0.35 - 1.00	0.294 - 0.327	0.760 - 1.188	50.37 - 71.33	14.70 - 26.10	1.23 - 2.18	270° for 12 runs 90° for 3 runs	57 - 72	67 - 82
46 - 60	0.77	Square	0.35 - 1.00	0.289 - 0.324	0.733 - 1.210	50.16 - 71.62	15.20 - 35.00	1.27 - 2.92	315° for 6 runs 45° for 9 runs	45 - 60	55 - 70
61 - 75	1.00	Circular	0.35 - 1.00	0.288 - 0.335	0.751 - 1.113	51.39 - 72.78	4.30 - 15.30	0.36 - 1.28	270° for 11 runs 90° for 4 runs	50 - 66	60 - 76
76 - 90	1.00	Square	0.35 - 1.00	0.290 - 0.324	0.731 - 1.100	49.25 - 71.15	9.50 - 22.30	1.82 - 3.27	315° for 7 runs 45° for 8 runs	42 - 59	52 - 69

3. EFFECT OF *C* AND *U* ON Y_S AT CIRCULAR PIER WITHIN LONG CONTRACTION

Variation of y_s around circular piers in long contraction shows a similar trend observed in pier scour experiment as reported by Debnath et al. 2010; 2011 for different U and C in bed sediments. Figures 3(a – c) present the plot of non-dimensional maximum equilibrium scour depth $sy\hat{}$ ($Dyys=\hat{}$) as a function of C at U_1, U_2 and U_3 respectively for varying b_c i.e at $b_c = 0.44$; 0.77; 1.00. For all the runs the minimum value of y_s recorded at $C = 0.50$ and the maximum at $C = 1.00$, except for run no. 6 and run no. 11, where the maximum y_s for $C = 0.35$ at U_2 and U_3 respectively for $b_c = 0.44$. It is interesting to note that here the effect of bc is prominently much higher than the consequence of flow velocity i.e. U. The rise of is significantly much greater with the fall of b_c. The shift of $sy\hat{}$ with incremental flow velocity i.e. from U_1 to U_2 and U_3 for a particular C is comparatively much lower than the shift of with the decrement of b_c.

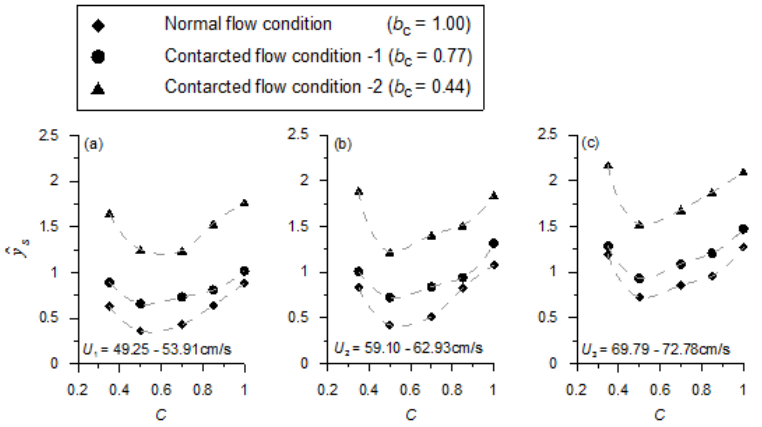

Figures 3(a-c) Variation of $\hat{}sy$ as a function of C for different cb in the case of circular pier; (a) for the experimental runs at U_1; (b) for the experimental runs at U_2 (c) for the experimental runs at U_3

Location of y_s as recorded at the side of the pier i.e. at 90° or 270° scales for all the runs with circular pier shows a similarity with as made by Debnath and Chaudhuri 2010. The experimental run time to reach the equilibrium scour condition, T_c, is gradually increased with the rise of y_s.

4. EFFECT OF *C* AND *U* ON Y_S AT SQUARE PIER WITHIN LONG CONTRACTION

Figures 4(a – c) shows the plot of *sy*ˆ versus *C* for square pier embedded in long contraction. The variation of with C resembles closely with the variation of for circular pier within long contraction.

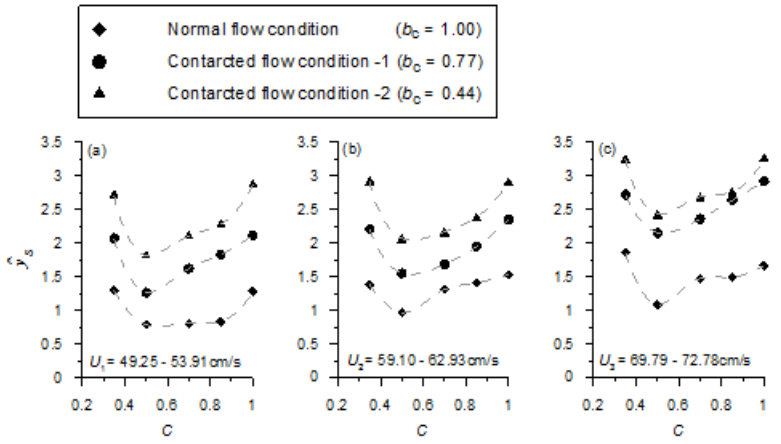

Figures 4(a-c) Variation of ˆ*sy* as a function of *C* for different *cb* in the case of square pier; (a) for the experimental runs at U_1; (b) for the experimental runs at U_2 (c) for the experimental runs at U_3

The significant difference is the location of maximum equilibrium scour depth (*sy*), for square pier was noted either along 45° or 315° scales for almost all the experimental runs except the run no. 76 and run no. 77 with $C = 0.35$ and $C = 0.50$ at U_1, where noted at 225° scale. From the figures 4(a – c) it is r that rise of *sy*ˆ with the fall of b_c is quite gradual for the velocity range of U_1 and U_2 for all the sediment beds with varying *C*. At U_3 the normalized equilibrium scour depth,, for all the beds with different *C* show a sharp rise when b_c decreases from 1.00 to 0.77. This increase is much smaller for the change of b_c from 0.77 to 0.44. Narrowing of flow passage causes a rapid hike in the flow velocity and perturbation which in turn generate concentrated flow vortices and may results in increased side wall effect at higher flow velocity (*i.e.*, at U_3) can be a cause for this rapid increase of (figure 4.c) at $b_c = 1.00$ to $b_c = 0.77$. For a change in b_c (*i.e.*, from 1.00 to 0.77 and from 0.77 to 0.44) the gradient of for a particular *U* shows a significant similarity for all the different bed sediment characteristics for most of the runs.

5. EFFECT OF PIER SHAPE ON *sy*ˆ

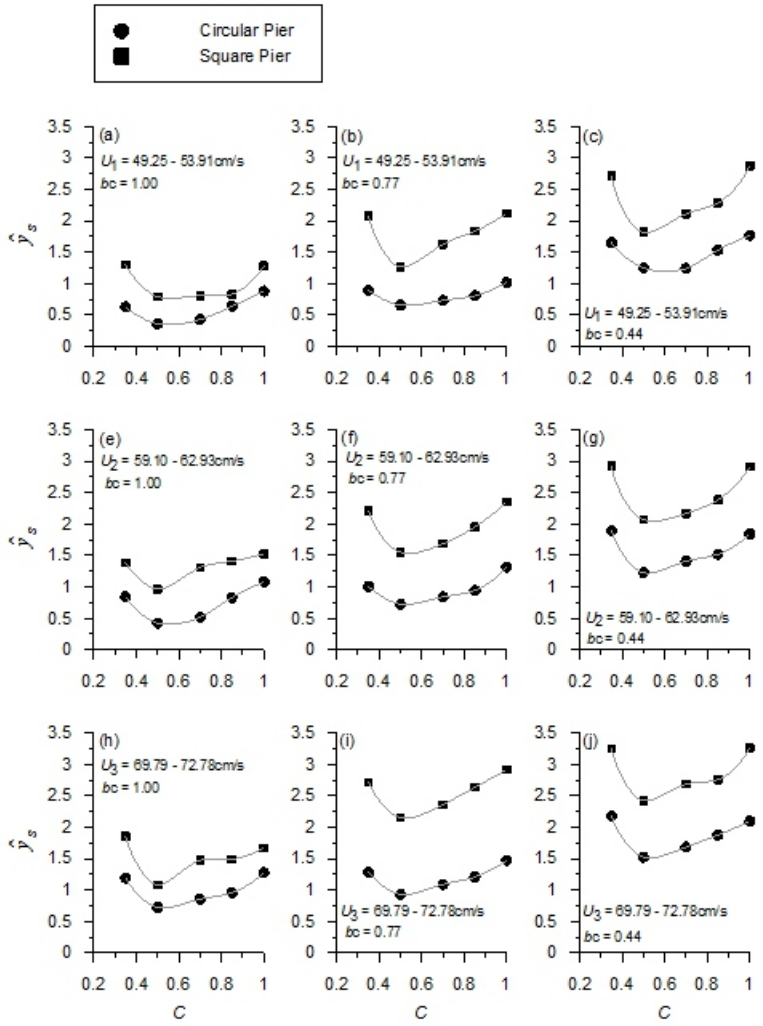

Figures 5(a-j) Variation of ˆ*sy* as a function of *C* for different *cb* in the case of circular and square pier for same flow velocity condition

Plots of *sy*ˆ against *C* at different *U* and varying values of b_c (Figures 5. a –j) for both the pier shapes shows a similar trend considering the effect of *C*. For all the runs the minimum value of observed at *C* = 0.50. The values of are substantially greater for the square pier than that of circular. These differences are gradually increased with the increase of *U* for all the bed sediment characteristics with varying *C*. For a particular bed characteristic i.e. mixed sediment bed with a certain *C*, the increase of with decreasing values of b_c dose not show any particular trend, though is higher in all the cases for lower value of b_c. It is also revealed from the plots that the variation of with *C* is more acute in case of square pier than circular one. The sinuosity of the plot of much greater for the runs with square pier especially at lower b_c and higher *U*. From the figures 5.b; 5.c; 5.d; 5.h; and 5.j clearly shows though the values of for square pier initially decreases with *C* up to 0.50 then it increased, the trend of increase not as smooth as circular pier but fluctuate to a considerable extent. Perhaps the development and propagation of flow

vortices responsible for the generation of scour hole at square pier was not very sequential as in the case for circular pier particularly in cohesive sediment beds, where the dislodgement of flocs and sediment grains is much complex and not solely depend upon bed shear stress (Mitchener and Torfs 1996; McAnally and Mehta 2002). Debnath and Chaudhuri (2010a, b) attributed this sharp change to the phenomenon that the scouring process involved different modes (as observed in camera): chunk-by-chunk, aggregate-by-aggregate to particle-by-particle. For a given approach flow velocity, bed shear stress (τ) reduced within the scour hole with increase in y_{st}. Up to a certain value of τ, the leading mechanism for the scour hole formation was by the rupture and transportation of chunks and aggregates from the sediment bed around the cylinder. As the depth of scour hole increased, the agents for scouring such as bed shear stress, horse shoe vortex, wake vortices (Ettema et al. 2006) reduced in intensity inside the scour hole and thereby did not have sufficient energy for the rupture of flocs / aggregates and the mode of erosion changed to particle-by-particle instead of aggregate-by-aggregate or chunk-by-chunk. Therefore, at higher flow velocity at lower value of bc the scour profiles were seen to be much irregular and corrugated around square pare compare to scour at circular pier. Dislodgement of large folcs of sediment at the initial stage of scouring is may be the prime cause for irregular scour shape at square pier.

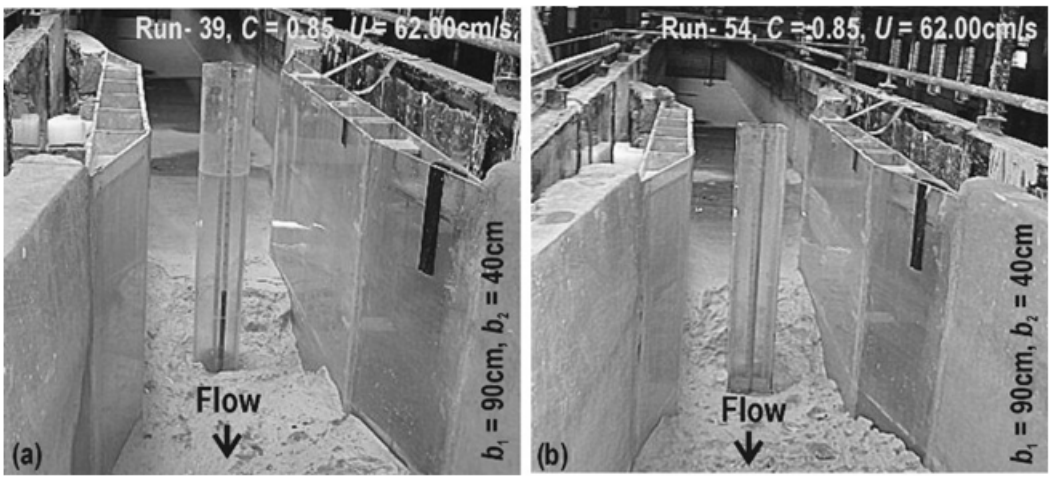

Figures 6(a-b) Photographs of equilibrium scour hole profiles (a) for the experimental run no. 54 around square pier (b) for the experimental run no. 39 around circular pier

Figures 6(a-b) shows the photographs of the equilibrium scour hole profile for the run no. 39 and 54 at U_2 (U = 62.00 cm/s) for b_c = 0.77. Through the photographs it is clear that surface roughness of the equilibrium scour hole is much higher for square pier than circular. Photographs also reveal the both up and downstream extension of scoured zone is higher for the square pier which extends beyond L. This obviously implies that the perturbation and energy of the flow vortices responsible for scouring at pier within long contraction is much higher in case of square pier.

6. EFFECT OF B_C ON $_{sy}\hat{}$

Effect of contraction ratio, b_c on $_{sy}\hat{}$ for different bed sediment with varying C has been shown in the figures 7 (a – j). Variation of $\hat{}_{sy}$ as a function of b_c for clay-sand mixed sediment beds with different C in three different velocity ranges, i.e in U_1, U_2 and U_3 for circular and square pier shows for all the velocity ranges with decreasing value of bc, increases for all bed sediments i.e. all C. The plots envisaged for circular pier the increase of is more acute for the change of b_c from 0.77 to 0.44 than its reduction from 1.00 to 0.77.

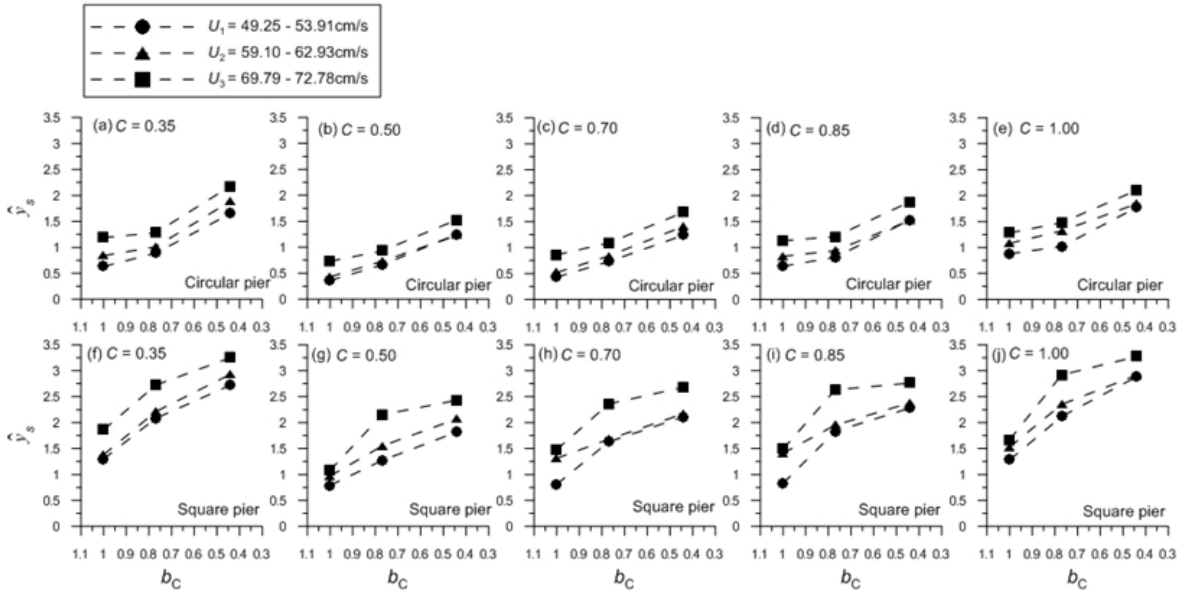

Figures 7(a-j) Variation of $\hat{}_{sy}$ as a function of b_c for clay-sand mixed sediment beds with different C in three different velocity ranges, i.e in U_1, U_2 and U_3 for circular and square pier

The relation is just vice versa for the runs with square pier where the gradient of rise of $\hat{}_{sy}$ is much higher at initial fall of b_c from 1.00 to 0.77. 44 than 0.77 to 0.44. For all the sediment beds the increase of with the falling value of b_c is much higher for the square pier rather than circular pier (figures 7 f-j). Considering the flow velocity, the increase of is significantly high for the velocity increase from U_2 to U_3 rather than U_1 to U_2 for all the bed condition and b_c. For square pier this rise is much prominent compare to the rise of $_{sy}\hat{}$ for circular pier. This may be due the increased concentration of flow vortices which ultimately resulted to energized perturbation at the constricted zone in between the side wall of the square pier and side wall of contraction. The decreased value of b_c probably caused a relatively smoother vortices and comparatively a lesser energy flow in case of circular pier, as revealed from the plots (figures 7 a-e) for all the sediment bed with varying C.

7. CONCLUSIONS

The paper reported new data on local scour in long contraction and pier scour embedded within that for clay–sand mixed cohesive sediment beds. It was observed that values of equilibrium scour depth y_s increased with the increase of C within the bed sediment up to a limit of $C = 0.50$ and decrease after that. It was also noted that flow velocity and contraction ratio plays a significant role on y_s, which is proportional with the flow velocity and reciprocal with b_c. Equilibrium scour depth at pier embedded within the long contraction increases sharply with the narrowing of the constricted zone i.e. with the decrease of b_c for all the bed sediment conditions. For circular pier the location of y_s was noted at the sides of the pier (i.e. either at 90° or 270° scale), where as for the square pier it wasnoted at the upstream facing corners of the pier (i.e. either at 45° or 315° scale), The change of normalized equilibrium scour depth $\hat{}sy$ with the change of U are much higher for square pier than the changes noted in case of circular pier. Considering the effect of b_c on it was revealed form the plots that the for circular pier the increase of is more acute for the change of b_c from 0.77 to 0.44 than its reduction from 1.00 to 0.77. The relation is just vice versa for the runs with square pier. The increase of is significantly high for the velocity increase from U_2 to U_3 rather than U_1 to U_2 for a particular b_c.

REFERENCES

Briaud, J. L., Chen, H. C., Li, Y., Nurtjahyo, P., and Wang, J. (2003). Complex pier scour and contraction scour in cohesive soils." NCHRP Rep. Transportation Research Board, Washington, D.C., 24-15,

Debnath, K. and Chaudhuri, S. (2010). Laboratory experiments on local scour around cylinder for clay and clay-sand mixed beds, Engineering Geology, 111, 51-61.

Debnath, K. and Chaudhuri, S. (2010). Bridge pier scour in clay-sand mixed sediments at near threshold velocity for sand, Journal of Hydraulic Engineering, ASCE, 136(9), 597-609.

Debnath, K. and Chaudhuri, S. (2012). Local scour around non-circular piers in clay–sand mixed cohesive sediment beds, Engineering Geology, 151, 1-14

Ettema, R., Kirkil, G., and Muste, M. (2006). Similitude of large-scale turbulence in experiments on local scour at cylinders. Journal of Hydraulic Engineering, 132(1), 33-40.

McAnally, W. H., and Mehta, A. J. (2002). Significance of aggregation of fine sediment particles in their deposition. Estuarine, Coastal and Shelf Science, 54, 643-653.

Mitchener, H. J., and Torfs, H. (1996). Erosion of mud/sand mixtures. Coastal Engineering, 29, 1-25.

Raiker, R. V., and Dey, S. (2005). Clear-water scour at bridge piers in fine and medium gravel beds Canadian Journal of Civil. Engineering, 32, 775-781.

Gill, M, A. (1981). Bed erosion in rectangular long contraction. Journal of Hydraulic Engineering, ASCE, 107(3), 273-284.

Koruma, S. (1966). Equilibrium depth of scour in ling contraction. Journal of Hydraulic Division, ASCE, 92(5), 17-38.

Laursen, E. M.(1963). An analysis of relief bridge scour. Journal of Hydraulic Division, ASCE, 89(3), 93 – 118.

Lim, S. Y. and Cheng N. S., (1998) Scouring in long contraction. Journal of irrigation and drainage engineering, ASCE, 124(5), 258-261

Multiple Inflow River Flood Routing Using ANN

Bahnisikha Das[1], Ruhul Amin Mozumder[2], B S Sil[3]
[1]*M.Tech Scholar, Civil EnggDeptt, NIT Silchar, Silchar and 788010, India*
[2]*Ph.D Scholar, Civil EnggDeptt, NIT Silchar, Silchar and 788010, India*
[3]*Asst. Prof, Civil EnggDeptt, NIT Silchar, Silchar and 788010, India*
Email: bahnisikha.das513@gmail.com

A B S T R A C T

The Muskingum flood routing method is one of the most popular routing procedure for estimation and forecasting of flood which is being widely used by the researchers and engineers throughout the world. The application of two parameter based Muskingum model is valid only for single inflow flood routing without any lateral inflow into the routing reach. However, normally a river is fed by a number ofbranch channels or rivulets at various upstream points. So, the single inflow-outflow Muskingum model cannot be applied in such situation. To overcome this problem, artificial Neural Network (ANN) has been applied in a river system considering inflow from various upstream rivers with a common outflow section. A simple static ANN model have been developed using concurrent discharge data. The model is applied in Mississippi River network starting from St. Louis, Montana to downstream section at Thebes, Illinois. In this reach, from St. Louis to Thebes, in the Mississippi river, a total of six lateral inflows confluence to the main river at different locations. Using ANN model, considering water discharge asinput from all the upstream sections, water discharge at the most downstream section, Thebes is computed. Statistical performance analysis of the estimated data shows that ANN can be efficiently used for estimation of flood flow considering multiple inflows.

Keywords: flood routing, ANN, Muskingum, multiple inflows.

1. INTRODUCTION

River flood routing is of extreme importance to water resources engineers and planners. Muskingum flood routing method is the most popular routing procedures. Muskingum procedure is based on the concept that the storage in the reach through which a flood is being routed is proportional to a weighted sum of inflow into and outflow out of the reach. The basic Muskingum formulation is applicable to a single channel reach bounded by an inflow and outflow gauging site and having no lateral inflows into the routing reach. However in natural channels, the presence of lateral inflow is very common and hence the Muskingum method is not applicable in such situation.

In this paper a new extended model for flood routing in a natural channel with gauged multiple tributaries is proposed. The model aggregates the tributary flows and the main channel inflow into an equivalent single

inflow at a characteristic point in the basin. The parameter representing the relative contribution of the member channel inflows in constituting the single equivalent inflow was estimated using artificial neural network. The performance of this model was compared with the observed values. The results obtained shows that the model can be used effectively and efficiently to estimate the optimal parameter values of the multiple inflows routing model.

An artificial neural network (ANN) has the distinctiveness of parallel link, error correction, and nonlinear transfer and is arising technique for the flow and association of information. It is constructed to obtain a forecast of system reaction without attempting to reach an understanding of or provide close into the nature of the phenomena that are represented (Haykin 1994, Fausett 1994, Hornik 1989, Fahlamn 1989, Rumelhartet al. 1986, Rogers and Lamarsh1992). It is a tool for nonlinear input–output mapping, which usually consists of input, output, and layers of hidden units or elements called neurons. This paper is concerned with the application of the artificial neural network to water flow problems in a complex river system. The objective of this study is to develop an ANN river system model for simulating and predicting flow and in a river system and to demonstrate the practical capability and usefulness of the ANN technique. The model utilizes the real river system being simulated as the ANN architecture and incorporates the physical behavior and internal conditions of the system. The integration of physical functions into the model and the use of an actual river network for ANN construction make it possible to have an appropriate or optimum architecture for ANN modeling and make it easier for the engineering community to understand the technique and interpret results. The model is intended for real-time prediction of flow in a complex waterway network with less data required for topographical and morphometric information than a conventional hydrodynamic model without compromising modeling accuracy.

2.METHOD

2.1 Overview of ANN

An ANN is simplified mathematical representation of the biological neural network. It has the skill to learn from examples, identify a pattern in the data, adapt solution over time, and process information quickly. The application of ANN to water resource problems is rapidly gaining popularity due to their enormous power and potential in mapping of non linear system data.

A water resource system may be nonlinear and multivariate and the variables involved may have compound interrelationships. Such problems can be competently solved using ANNs. The processes that involve several parameters are easily amenable to neurocomputing.

An ANN consists of a number of data processing elements called neurons or nodes that are grouped in layers. Each neuron is connected to other neurons by means of direct communication links. The neurons in one layer are not connected among themselves. The input layer neurons receive the input vector and transmit the values to the next layer of processing elements across connections. This process is continued until the output layer is reached. The data passing through the connections from one neuron to another are multiplied by weights that control the strength of a passing signal. The weights represent information being used by the net to solve a problem.Each neuron multiplies every input by its interconnection weight, sums the product, and then passes the sum through an activation (or transfer) function to produce its result. The desired output is achieved by adjusting the weights on the links between the neurons and calculating the value of error function for a particular input and then back-propagating the error from one layer to the previous one (Rumelhartet al. 1986). This type of network in which the data flows in one direction is called the feed forward network(Rumelhartet al.1986, White 1990, Gallant and White 1992).Among many ANN structures, the most widely used one in the area of hydrology is the multilayer, feed forward network (Rumelhartet al. 1986).

2.2ANN Learning

The process of determining ANN weights is called learning or training and is similar to calibration of a mathematical model. The ANNs are trained with a training set of input and known output data. At the beginning of training, the weights are initialized either with a set of random values or based on some previous experience. Next, the weights are systematically changed by the learning algorithm such that for a given input the difference between the ANN output and actual output is small. The ANN learning process is terminated when this difference is less than a specified tolerance. In general, there are two additional termination procedures that are commonly used: (1) when the weights are updated a maximum number of times and (2) when the error calculated for a separate test dataset begins to increase, i.e., by cross-validation.

The most widely used learning rule for ANNs or multilayer perceptron is the error back-propagation (BP) algorithm developed by Rumelhart and others (1986) (Tchaban et al. 1998, Bishop 1995). The BP algorithm is based upon the generalized delta rule. In BP processes, all nodes change their weights based on the accumulated derivatives of the error with respect to each weight. A set of inputs and outputs is selected from the training set, and the network calculates the output based on the inputs. This output is subtracted from the actual output to find the output layer error. The error is back propagated through the network, and the weights are suitably adjusted. This process continues for the number of prescribed sweeps or until a prescribed error tolerance is reached. The mean square error over the training samples

is the typical objective function to be minimized. After training is completed, the ANN performance is validated and implemented for its intended use. An ANN is better trained when a wider range of environmental scenarios is used, under which input data are collected. If the model is trained using a dataset that contains a limited range of values, it may perform poorly when encountering events having previously unobserved values. The failure to generalize may limit its use as a tool in applications where the data available for calibration is unlikely to cover all possible scenarios. Imrieet al. (2000) presented a methodology for improving the generalization performance of an ANN model by adding a guidance system to a learning architecture and including a simple cross-validation procedure in ANN training. The method can produce models that generalize well on new data and extrapolate beyond the range of values included in the calibration range. Imrie et al. (2000) scaled river flow data so that the training data values lay between 0.2 and 0.8 or between 0.1 and 0.9. However, reducing the range of the scaled values further may lead to loss of information and a poorer overall network performance (Imrieet al. 2000).

The determination of optimal network architecture is a part of the learning strategy (Fahlman and Lebiere 1990). The number of input, output, and hidden layer nodes depends on the problem being studied. There are no fixed rules about the number of nodes in the hidden layer. However, if the number of nodes in the hidden layer is too small, the network may not have sufficient degrees of freedom to learn the process correctly. If the number is too high, the training will take a long time and the network may sometimes over fit the data (Karunanithiet al. 1994). The configuration that gave the minimum mean square error (MSE) was selected as the ANN structure (Jain and Chalisgaonkar 2000). In this study, a river system is modeled by an ANN configuration, which is based on the structure of the river network, so that the difficult and time-consuming practice in finalizing the hidden layer structure can be avoided.

2.3 ANN Representation of a River System

A river system is composed of intertwining channels, tributaries, lakes, and other water bodies connected to each other. It may be nonlinear and multivariate, and the variables involved may have complex interrelationships. Such problems can be efficiently solved using ANNs as there are many similarities between a neural network and a river system. Therefore, it is reasonable to use an ANN model to simulate flow process in a complex river system.

A river system can be conceptualized according to research needs and the connection and interaction between water bodies. To meet the requirement for developing an ANN model for flow, some considerations or assumptions are made. The river network is represented by a system of interconnected nonlinear reservoirs. Upstream inflows to various water bodies are used as the model input and downstr-

-ream flow rates at a downstream station as the model output. It is assumed that there is no interaction, i.e., water exchange, between reservoirs in the same layer of the network. Interaction between reservoirs in the adjacent layers is represented by the weight, to which a zero is assigned if there is no exchange between two layers. This treatment makes the use of the similarity between the ANN and the river network. The nodes in the first and last layers of the network serve as input and output, respectively, and do not have storage capability. The nodes of the internal layers have storage functions through which there is water exchange. Reservoir storage-outflow function is nonlinear for water. Water conservation principle applies to all reservoirs in the river system.

With the above-mentioned assumptions and considerations, the simplified representation of a river network consists of three components: water inflow (sources) as input, internal reservoirs in parallel or series, and water outflow as output. A nonlinear relationship exists between the input to the first layer and the output from the last node. The water continuity equation is used for satisfying water conservation over the whole river system as well as at all nodes.

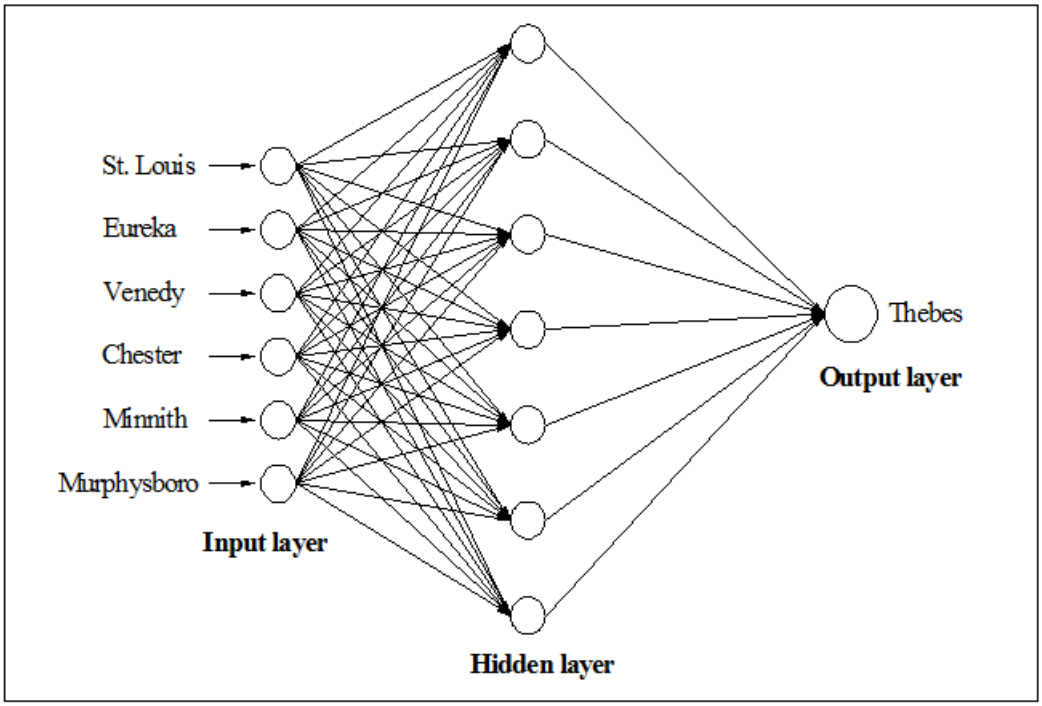

Figure 1 Three layer Feed-forward ANN

2.4 Development of ANN model for prediction of discharge

In the present study an ANN model was developed to predict the discharge of Mississippi River basin in the United States. The river has many tributaries in which the flow from various stations i.e. St.Louis (Montana), Eureka (Montana), Venedy (Illinois), Chester (Illinois), Minnith (Montana), Murphysboro (Illinois) etc meets at station Thebes (Illinois). The flowrate of the various gauging stations starting from

April 1, 1981 to September 30, 1981 is collected from USGS station. The ANN model was developed by considering discharge at St.Louis (Montana), Eureka (Montana), Venedy (Illinois), Chester (Illinois), Minnith (Montana) and Murphysboro (Illinois) stations as input and discharge at Thebes (Illinois) station as output. A multilayer feed-forward perceptron with one hidden layer was adopted in the present study. The transfer function at the hidden layer was tan hyperbolic tangent whereas transfer function at the output layer was pure linear. To find the optimum number of neurons in the hidden layer, the number of neurons in the hidden layer were varied from four (4) to fifteen (15). Before presenting to the network the data were normalized to fall in the range [-1, +1]. Data division was carried out by using 70% data for training and rest 30% for testing. A total of 183 data were used for developing ANN model for discharge prediction. The statistical parameters of training and testing data are presented in Table 1. Bayesian regularization was adopted as training algorithm for its better generalization to the training data. The ANN model was implemented in MATLAB R2013a environment. The performance function was set to be mean squared error (MSE). However the networks performance was also reported via two other statistical parameters namely mean absolute percentage error (MAPE) and linear co-relation coefficient (R). Statistical parameters MSE, MAPE and R are defined as follows

$$MSE = \frac{1}{n}\sum_{i=1}^{n}(x_m - x_o)^2 \quad (1)$$

$$MAPE = \frac{1}{n}\sum_{i=1}^{n}\frac{|x_m - x_o|}{x_o} \quad (2)$$

$$R = \frac{n(\sum x_m x_o) - (\sum x_m)(\sum x_o)}{\sqrt{\{[n(\sum x_m^2) - (\sum x_m)^2][n(\sum x_o^2) - (\sum x_o)^2]\}}} \quad (3)$$

where x_o and x_m are the observed data and predicted data respectively and n is the total number of data.

Table 1 Statistical parameter of training and testing data

Statistical parameter	Station name						
	St.Louis	Eureka	Venedy	Chester	Minnith	Murphysboro	Thebes
Training data							
Mean	6914.36	166.50	78.36	5206.86	63.79	1.64	7024.10
Standard deviation	2828.68	220.18	44.89	2596.77	79.93	4.30	2869.30
Maximum	13900.00	1160.00	177.00	14200.00	328.00	35.70	14800.00
Minimum	2440.00	26.70	3.40	2050.00	2.75	0.14	3030.00
Testing data							
Mean	6535.93	125.50	74.25	5179.26	73.90	1.24	7470.74
Standard deviation	2498.87	197.42	50.79	2097.34	96.96	1.71	2686.66
Maximum	14400.00	1100.00	176.00	12200.00	314.00	8.16	11900.00
Minimum	2540.00	28.90	3.57	2970.00	2.86	0.19	3090.00

2.5 Results and discussion of ANN model

The performance of the ANN networks with different number of neurons in the hidden layer is presented in Table 2. From the Table 2, it may be observed that MSE, MAPE & R value of testing data is optimum with seven (7) neurons in the hidden layer (highlighted in bold & Italic). MSE, MAPE & R values of training and testing data of the network with seven neurons in the hidden layer were found to be 1.03x106, 9.42% and 0.935 &, 1.12x106, 9.62% and 0.920 respectively. MSE, MAPE & R values of both training and testing data implied that the ANN model has successfully learnt and predicted the discharge. The weights and biases of the ANN model with seven hidden layers are presented in Table 3.Figure 2 shows the plot of observed discharge against the predicted discharge for training, testing and all data including training and testing. The performance of ANN model is presented in Figure 3. It may be observed from Figure 3 that MSE value started at a large value and decreased as the number of iteration (Epoch) increased. It is also observed from Figure 3 that by the 62nd iteration there was no over fitting in the data which suggests that Bayesian Regularization has successfully prevented over fitting of testing data.

Table 2 Performance of ANN model with different number of neurons in the hidden layer

Number of neurons in the hidden layer	MSE x 10^6			MAPE			R		
	All	Training data	Testing data	All	Training data	Testing data	All	Training data	Testing data
4	1.61	1.34	3.16	12.28	11.19	18.78	0.895	0.913	0.793
5	1.54	1.34	2.67	11.43	10.90	14.10	0.900	0.910	0.845
6	1.37	1.21	2.26	10.61	10.51	11.19	0.912	0.922	0.866
7	1.04	1.03	***1.12***	9.45	9.42	***9.62***	0.933	0.935	***0.920***
8	0.92	0.64	2.56	8.53	7.29	15.20	0.942	0.961	0.821
9	0.95	0.58	3.09	7.97	6.98	11.97	0.940	0.959	0.875
10	0.69	0.28	3.09	5.68	4.27	13.80	0.958	0.984	0.798
11	0.86	0.37	3.69	7.18	5.22	16.08	0.946	0.976	0.808
12	1.01	0.29	5.20	5.21	4.01	12.92	0.939	0.982	0.756
13	3.17	0.08	21.05	7.11	2.41	27.81	0.853	0.996	0.566
14	0.60	0.18	3.01	4.90	3.14	14.16	0.964	0.989	0.874
15	0.77	0.26	3.67	5.74	4.37	13.59	0.952	0.984	0.782

Table 3Weights and biases of ANN model with seven neurons in the hidden layer

Hidden neuron		1	2	3	4	5	6	7
Weights								
Station name	St.Louis	-0.4242	-0.1375	-0.3856	-0.0604	-0.2837	-1.7506	0.0475
	Eureka	1.8813	-2.5743	-1.1114	0.0648	2.5084	0.0208	3.1853
	Venedy	-0.8685	1.2929	-2.2101	1.5598	-0.3801	-0.3262	1.5660
	Chester	0.6017	2.0765	0.6184	2.2197	-0.6666	-1.7561	-0.6660
	Minnith	-0.7666	1.0701	1.7490	-0.4829	-0.9462	-0.7424	-0.5708
	Murphysboro	-0.6323	0.0056	0.4111	0.6828	0.0101	1.8463	-1.0195
	Thebes	-1.3247	1.7743	-1.5386	-0.9376	2.6868	-0.9197	-2.4968
Biases								
Hidden layer		0.1924	-0.8983	-0.6043	0.6729	0.6844	-1.0723	1.8239
Output layer		-0.1946						

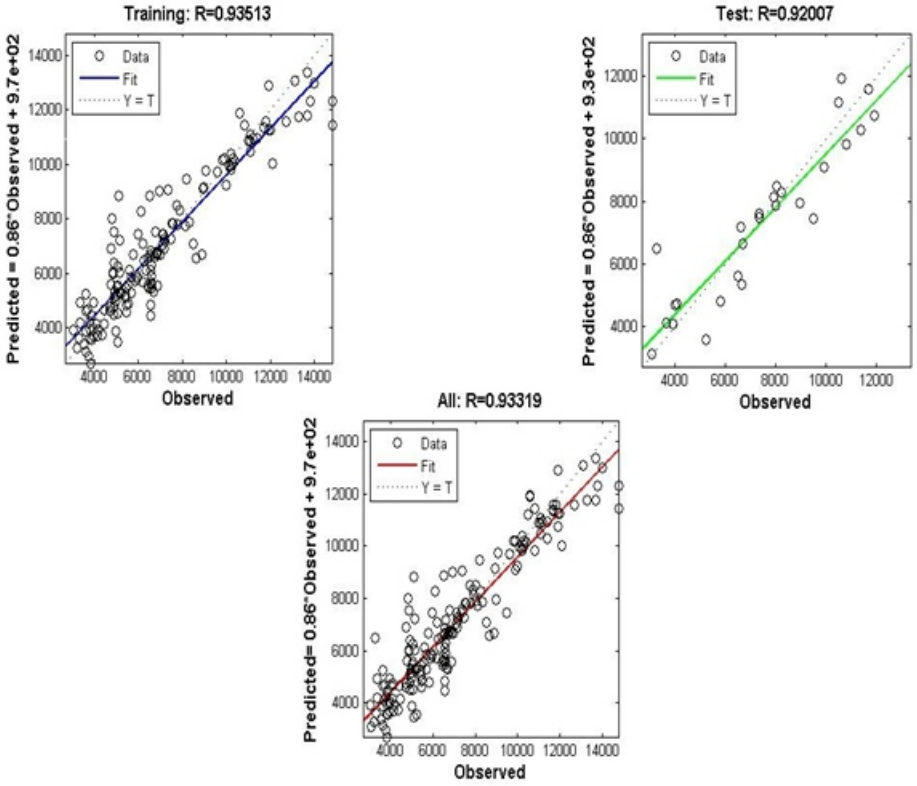

Figure 2 Observed discharge versus Predicted discharge

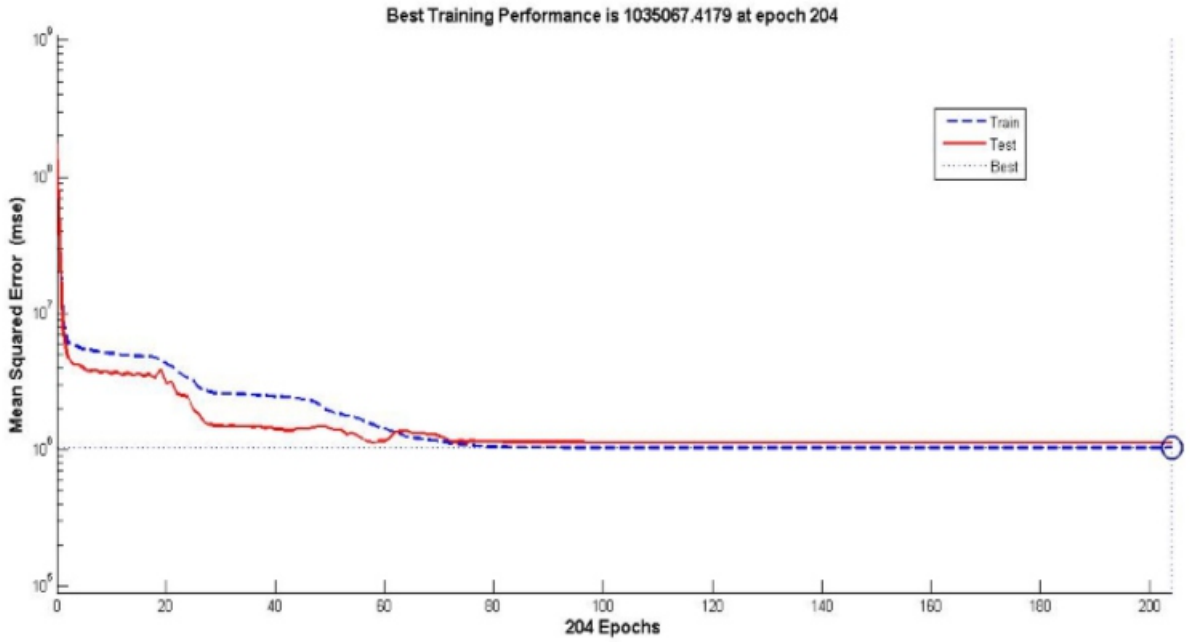

Figure 3 Performance of ANN model for discharge prediction

3. CONCLUSIONS

Flood routing of a river having multiple inflows cannot be carried out by Muskingum model since it is valid only for single inflow flood routing. Considering the similarity of the structure and the input-output relation between a neural network and a river system, the adoption of artificial neural network for simulating the water movement in a river network is adequate and practical. An advantage of using the ANN is that it can successfully model the unsteady flow behavior in a complex system of rivers.An ANN model has been developed by considering the water flow from St.Louis, Eureka, Venedy, Chester, Minnith and Murphysboro as input and water flow from Thebes as output of the Mississippi river. Model results and the field measurements matches well. It is concluded that the ANN model for river system is capable of describing the water flow processes having lateral entries.

REFERENCES

Bishop, C. M. (1995). Neural networks for pattern recognition. Clarendon Press, Oxford.

Fahlman, S. E., and C. Lebiere. (1990). The cascade-correlation learning architecture. Technical report CMU-CS-90–100, School of Computer Science Carnegic-Mellon University, Pittsburgh.

Fausett, L. (1994). Fundamental of neural networks. Prentice- Hall, Englewood Cliffs, New Jersey.

Gallant, A. R., and H. White. (1992). On learning the derivatives of an unknown mapping with multiplayer feed forward networks. Neural Networks 5:129–138.

Haykin, S. (1994). Neural networks: a comprehensive foundation. Macmillan, New York.

Hornik, K. (1989). Multilayer feed forward networks are universal approximations. Neural Networks 2:359–366.

Imrie, C. E., S. Durucan, and A. Korre. (2000). River flow prediction using artificial neural networks: generalization beyond the calibration range. Journal of Hydrology 233(1–4): 138–153.

Jain, S. K., and D. Chalisgaonkar. (2000). On setting up stage discharge relations using ANN. Journal of Hydrologic Engineering 5(4):428–433.

Karunanithi, N., W. J. Grenney, D. Whitley, and K. Bovee. (1994). Neural networks for river flow prediction. Journal of Computing in Civil Engineering 8(2):201–220.

Rogers, J. L., and W. J. Lamarsh. (1992). Application of a neural network to simulate analysis in an optimization process. Proceedings, Artificial Intelligence in Design '92, Kluwer Academic, Boston, pp. 739–754.

Rumelhart, D. E., J. L. McLelland, and PDP Research Group. (1986). Parallel distributed processing, explorations in the micro structure of cognition, Vol. I: Foundations, MIT Press, Cambridge, Massachusetts.

Tchaban, T., M. J. Taylor, and J. P. Griffin. (1998). Establishing impacts of the inputs in a feed forward neural network. Neural Computing Application 7:309–317.

White, H. (1990). Connectionist nonparametric regression: multiplayer feed-forward networks can learn arbitrary mappings. Neural Networks 3:535–549.

Transient Analysis For Detection Of Unauthorized Branching In A Single Pipeline

Prabhat Kumar[1], Pranab K. Mohapatra [2]
[1] *PhD, IIT Gandhinagar VGEC Campus, Chandkheda, Ahmedabad- 382424, India*
Email:prabhat.k@iitgn.ac.in
Mobile No.: +91 9662421412
[2] *Professor, IIT Gandhinagar VGEC Campus, Chandkheda, Ahmedabad- 382424, India*
Email:pranabm@iitgn.ac.in
Mobile No.: +91 7600793659

ABSTRACT

Unauthorized Branching (UB) are often encountered in a piping networks such as water distribution, irrigation and oil/gas transporting system. There is enormous amount of losses in the pipe network due to the UB. Therefore, it is important to detect such UB connection in a piping system. Traditionally, the condition of pipeline networks has been monitored by a distributed set of pressure sensors, flow meters, and valve sensors. These sensors can monitor condition of valves, the presence of blockages/leaks and UB. However, multiple sensors are required to monitor a complex pipe network and thus the approach is costly and time consuming. On the other hand, transient based techniques have already been proven to be an efficient alternative to detect leaks and blockages in a piping network. The present work proposes that few transient measurements at one point can keep track of the system conditions and can be used to locate the UB. A simple reservoir-pipe-valve system with a single branching is considered herein to demonstrate the UB detection technique. Transient is created by sudden closure of the valve situated at downstream end of the main pipeline. The transient analysis is performed by solving the one-dimensional partial differential equations for pipe flow, by method of characteristics (MOC). A steady state friction model is used in the simulation. Time history of the pressure head at a point near the valve is studied to detect the UB. Results suggest that there is substantial drop in the time history of pressure head due to branching. This drop in pressure head is characterized by time of pressure drop (T_P) and magnitude of the pressure drop (ΔP). The location and the length of UB are predicted by T_P and ΔP, respectively. The results shown in this study are valid for a single pipeline with single branching. Further research is required to generalize the model for a piping network. The results presented herein are numerical by nature which require further validation through experimental results.

Keywords: Transients, Unauthorized branching in a pipeline, Water hammer

1. INTRODUCTION

Transient based method for fault detection are promising because they are noninvasive, inexpensive, simple to perform and can give information about the condition of pipeline. Transient measurements can keep track of the operation of the system. They can monitor the operation of pumps and valves also locate the possible leaks and unauthorized use (Liggett and Chen 1994). Though recently much attention has been given in detection of leaks and blockages in a piping system, little research has been done regarding the detection of unauthorized branch (UB) in a system by means of transients.

Annually hundreds illegitimate cut-ins with the purpose of theft of water and oil/gas products are reported. The level of the loss from these infringements is huge. It is advised that as far as possible, laying of the pipe should be done beneath the ground to protect the pipeline from tampering and unauthorized use. However, due to practical constraints it is not possible to keep the entire pipe underground and many times valves installed in the pipes get exposed. This gives an opportunity for UB to be set in the main pipeline.

In this paper, using transient as a tool to detect such UB in a system is investigated. Numerical experiments are conducted on a typical Reservoir-pipe-valve system and effect of UB in this system is analyzed. Transients are created by fast and complete closure of the downstream valve-1(Figure-1).Variation in pressure signals are simulated by varying the UB size and position along the main pipeline. Finally, it has been shown that the presented procedure gives conclusive results for a single main pipeline system.

2. UNDERLYING CONCEPT

When fluid flow in a pipe is suddenly stopped by a valve, (or flow is varied by any other means) pressure waves are created. These waves travel along the pipe until they reach a feature (Leak, Blockage, UB etc.) in the pipe network, where the wave is partly transmitted, and partly reflected back toward the source. Some of the wave energy is lost in the form of a pressure loss (Lighthill 2001). A pressure transducer can detect this pressure signal as the wave first traverses it and then again as it returns after having been reflected. If the speed of the wave a in the fluid is known, and the time t between the two passes of the wave at the pressure transducer is recorded, then the distance l to the point of reflection is half the product of the wave speed and the travel time

$$l = \frac{a \, . \, t}{2} \qquad (1)$$

If the pipe is flexible, (which is the case of most of the UB) the speed of sound is significantly less. Above method can be applied for the estimation of location of any feature in the piping system, however, the discussion here is limited to the evaluation of location of an UB.

3. GOVERNING EQUATIONS AND NUMERICAL SCHEME

Pressure transients in pipe systems are described by the well-known water hammer equations—the continuity and momentum equations. Classical mass and momentum equations for one-dimensional

(1D) (Chaudhry, 1987) water-hammer flow has been used in the present study. In most engineering applications, the convective acceleration are negligible and the basic hyperbolic differential equations of unsteady pressurized flows, can be written as

$$a^2 \frac{\partial Q}{\partial x} + gA \frac{\partial H}{\partial t} = 0 \quad (2)$$

$$\frac{\partial Q}{\partial t} + gA \frac{\partial H}{\partial x} + RQ|Q| = 0 \quad (3)$$

where x = distance along the pipe axis (m); t = time (s); A = cross-section flow area (m^2); Q = discharge (m^3/s); H = piezometric head (m);; g = gravitational acceleration (m/s^2); a = wave speed (m/s). R = f / (2DA).f= friction factor .D=Diameter of the pipe. Equation 2 and 3 are hyperbolic partial differential equation which doesn't have exact solution, hence some numerical method is required to solve them. These equations can be solved by several numerical methods. One of the popular methods, Method of Characteristics (MOC) is adopted in this paper. For the solution of 1D hydraulic transient, MOC has become extensively used, having proven to be better than other methods due to simplicity in programming and efficiency of results. (Chaudhary 1987; Wylie 1993; Almeida1992). Before closure of the valve-1 steady state conditions prevails in the system. At the internal nodes the positive and the negative characteristics equations are solved simultaneously to get the discharges and head values at the next time step. However, at the boundaries only one characteristic equation is available. Extra boundary conditions such as discharge at valve-1=0 (at all the time) and head at the reservoir node=$H_{reservoir}$ at all the time are applied.

4. THE SYSTEM

In the present numerical test a classic Reservoir-Pipe-Valve system has been used (Figure-1). A MATLAB code is written in which classical 1-D water hammer equations are solved using Method of characteristics. Transients have been created by instantaneous closure of valve-1 at the downstream end. Simulated results for the pressure at the downstream end is used to analyze the piping system. The constant head reservoir maintains a head of 25m at the upstream end. An UB of length L_{ub} = 300m is introduced in the pipeline and its effect on the pressure reading is assessed for different location and different sizes of UB. The Length, L_{mp} and diameter D_{mp} of the main pipeline is taken as 1250 m and 0.2 m respectively. A friction factor of 0.03 has taken for both the pipes.The other parameters of the system are presented in Table-1.

Table-1: Piping system Parameters

S No.	Pipetype	Length(m)	Diameter (m)	Wave Spped(m/s)	Friction Factor
1	Mainpipe	1250	0.2	1000	0.03
2	UB	300	varies	300	0.03

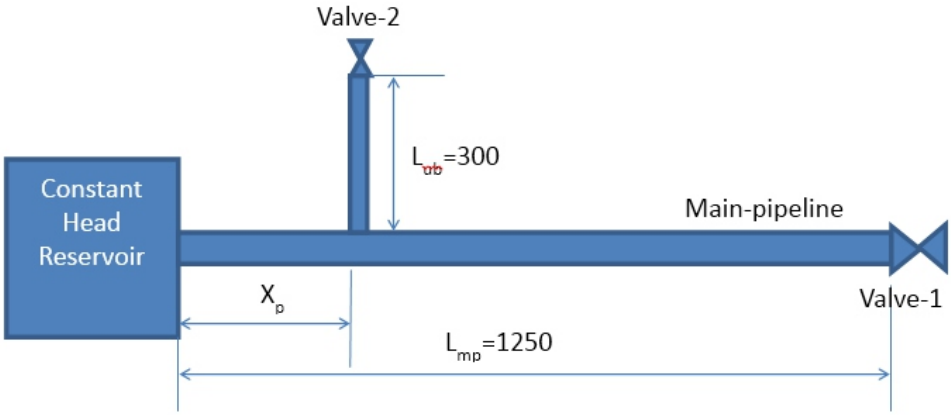

Figure-1: Schematic diagram for the piping system with UB

5. RESULTS

5.1 Pressure trace at the downstream end

Figure-2 shows the comparison of pressure signals at downstream end for two cases. In first case there is no UB in the system and for other case an UB is present at 250m from the reservoir (X_p = 250m).

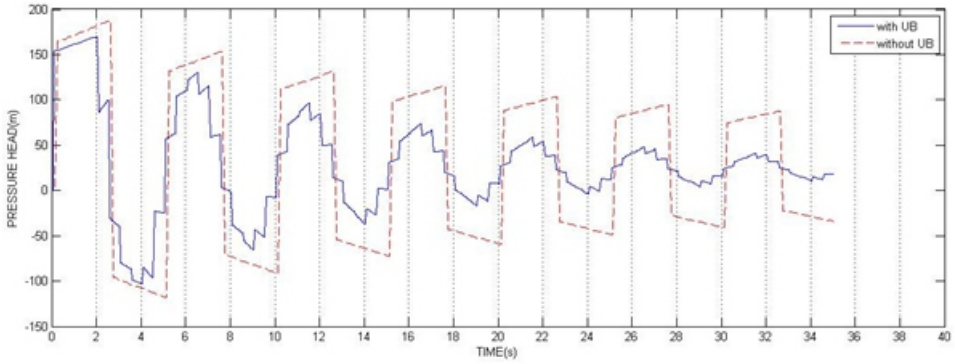

Figure-2: Pressure signals at the downstream end with and without UB

It can be observed in Figure-2 that for the case of UB not only the pattern of the signal changes, but also the rate of decay of signals increases. Both these attributes may be because of the presence of UB. In case of UB, multiple reflections and transmission occur at the junction, due to which many pressure waves can be observed simultaneously. Though researchers have tried to decode the whole signal produced by multiple reflections, (Beck et. al. 2005) only the initial phase of the signal is used in the present study.

5.2 Effect of location and size of UB

5.2.1 UB location

Pressure signals at the downstream valve-1 are obtained for four different locations of UB (Table-2). As the location of UB is changed, the piping system is modified and the initial steady state flow in the pipelines are varied. The values of discharges in the pipe according to X_p have been shown in Table-2. In all the numerical runs the diameter of the UB, (D_{ub}) was kept constant at 0.1m. The UB location and time are represented by non-dimensional parameter, $\delta = X_p/L_{mp}$ and $\Theta = (T_p)/(L_{mp}/a)$ respectively.

Table-2: Variation with different X_p values (constant D_{ub}=0.1m)

No. of Run	Xp(m)	δ=Xp/Lmp	Steady State Discharge in the pipes			Θ=(Tp)/(Lmp/a) (read from the signal)
			Q_{01} (m^3/s)	Q_{02} (m^3/s)	Q_{03} (m^3/s)	
1	250	0.2	0.0626	0.0153	0.0473	1.6
2	500	0.4	0.0580	0.0127	0.0453	1.2
3	750	0.6	0.0546	0.0101	0.0445	0.8
4	1000	0.8	0.0522	0.0072	0.0450	0.4

Figure-3 shows different times of drop of pressure (Θ) with different values of δ. The values of Θ for different runs are presented in Table-2.

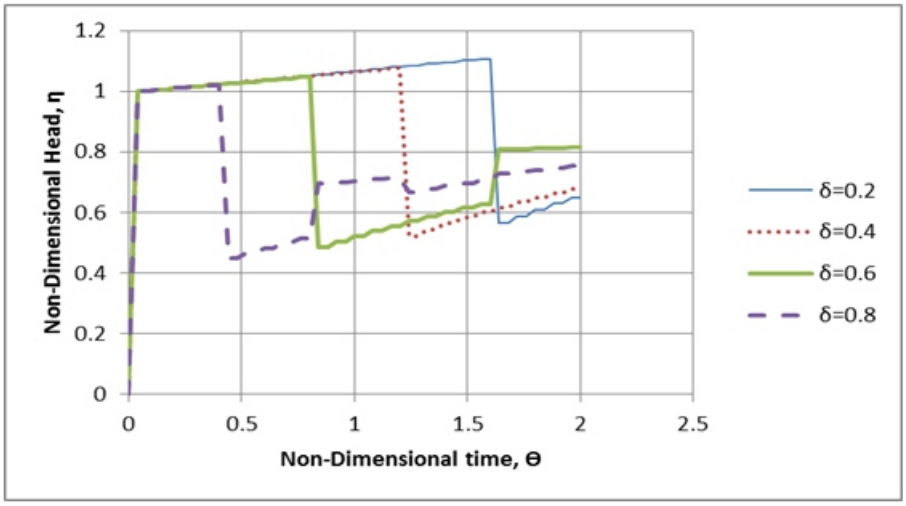

Figure-3: Effect of UB location on pressure head

It can be observed that as the value of δ is increased, the time of drop of pressure decreased linearly. This was expected since as δ increases, the UB comes closer to the pressure measuring point and the effect of reflected wave is observed much earlier. Figure-4 shows the variation of Θ with δ. The trend-line observed was

$$\theta = -2\delta + 2 \quad (4)$$

with a R-squared value of 1.

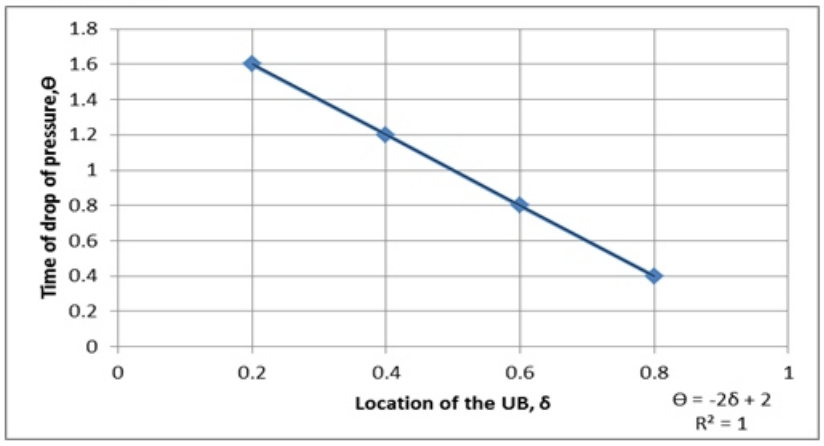

Figure-4: Prediction of the UB location

5.2.2. Variation with UB size

Pressure signals at the downstream valve-1 are obtained for different sizes (non-dimensional diameter $d^*=D_{ub}/D_{mp}$) of UB. Again, as the diameter of UB is changed, the initial steady state flow in the pipelines are different. The values of discharges are shown in Table-3. In all the numerical runs X_p is kept constant at 250m.The value of drop in pressure (ΔP), is shown in Table-3. Results for non-dimensional pressure drop, $\Delta\eta = (\Delta P)/(a.\Delta V/g)$ is presented.

Table-3: Variation with different UB diameter (D_2) (Constant X_p=250m)

No. of run	D_2 (m)	$d^*=D_2/D_m$	Steady State Discharges in the pipes Q_{01} (m^3/s)	Q_{02} (m^3/s)	Q_{03} (m^3/s)	$\Delta V=Q_{03}/A_{mp}$ (m/s)	Pressure drop ΔP(m)	Non-dimensional pressure drop $\Delta\eta=(\Delta P)/(a.\Delta V/g)$
1	0.050	0.250	0.0531	1.5987	0.0502	1.5987	27.8281	0.1707
2	0.075	0.375	0.0569	1.5668	0.0492	1.5668	55.6932	0.3487
3	0.100	0.500	0.0626	1.5063	0.0473	1.5063	83.2697	0.5423
4	0.125	0.625	0.0700	1.4267	0.0448	1.4267	105.8864	0.7281
5	0.150	0.750	0.0780	0.0367	0.0413	1.3152	120.1834	0.8964
6	0.175	0.875	0.0858	0.0486	0.0372	1.1847	126.0481	1.0437

Figure-5 depicts different magnitude of pressure drops with change in UB diameter. It is observed that as the diameter of the UB is increased, the drop in pressure is also increased. However, all the drops occurred at Θ=1.6. Figure-6 shows the variation of non-dimensional pressure drop (Δη) with non-dimensional diameter of UB (d*). A linear trend-line is fitted through the data who's R^2 = 0.9981.The equation of the trend-line is

$$\Delta\eta = 1.4157.d^* - 0.1747 \quad (5)$$

Equation (5) may be used to predict the diameter of UB.

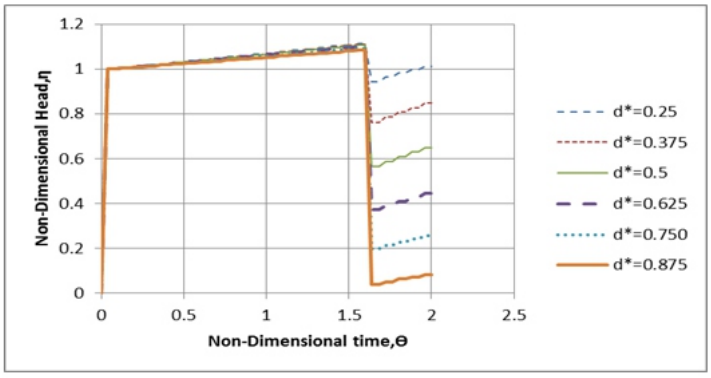

Figure-5: Pressure signal drop at Θ=1.6 for various diameter of the UB

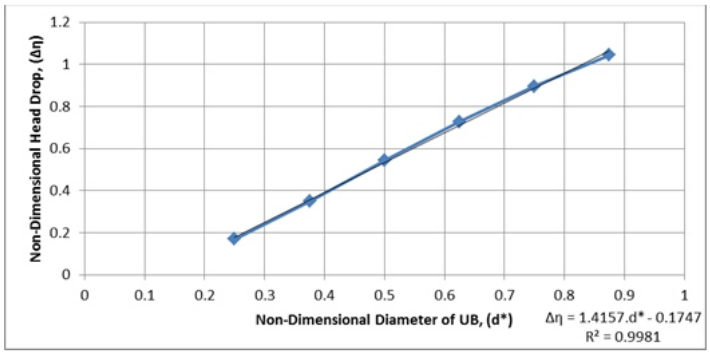

Figure-6: Variation in the drop of pressure with the diameter of the UB

6. DETECTION PROCEDURE

The parameters which are detected using the current methodology are the location of UB and its diameter. The detection procedure is described in the following steps.

Step-1: System parameters are noted.

Step-2: The transients are created on the field by instantaneous closure of the valve-1 and the pressure signal at the same point is recorded. The recorded signal is used as an input for the UB detection procedure.

Step-3: The time of first drop of pressure head (ΔT) and the magnitude of head drop (ΔP) are measured from the recorded signal. Convert these two parameters to their non-dimensional form Θ and δ respectively.

Step-4: Use these two non-dimensional parameters in equations (4) and (5) to calculate the non-dimensional location and diameter of the UB. Convert these non-dimensional values to get the location and diameter.

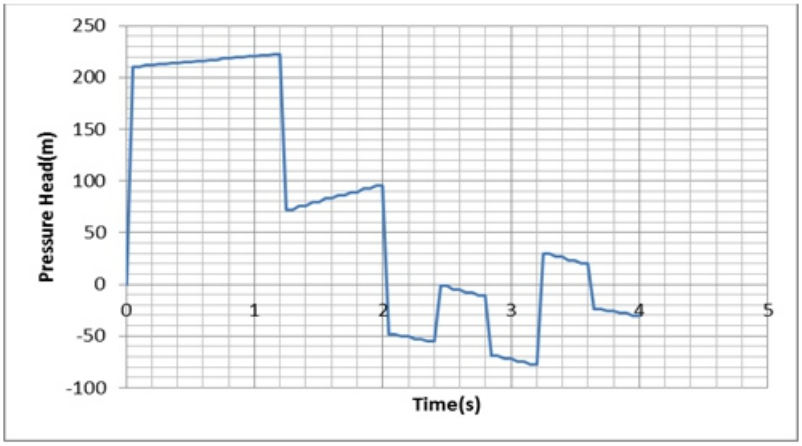

Figure-7: Synthetic Pressure signal for inverse analysis used in the Example

6.1 An Example

An example is used to demonstrate the above detection procedure. To evaluate the authenticity of equations (4) and (5), a system with different dimensions are used in the example. A 1000m pipe is used as the main pipeline which is connected to a 30m constant head reservoir at the upstream head and to a valve (valve-1) at the downstream end. A synthetic pressure signal (Figure-7) corresponding to X_p=400m (unknown) and D_2=180mm (unknown) is generated and used as an input to determine the UB characteristics. The pressure signal is shown in Figure-7. Step by step procedure as mentioned in section-6 can be used to determine the unknown parameters.

Step-1 and 2: System parameters are noted.

Table-4: The known parameters in the example

Main pipelength	Main pipe diameter	Wave speed	Constant Head	Steady State discharge at valve-1	Time of first drop (read from signal)	Magnitude of first drop (read from signal)
L_{mp}=1000m	D_{mp}=300mm	a=1000m/s	H_0=30m	Q_{03}=0.146m^3/s	1.2s	(220-70) = 150m

Step-3:

$$\Delta T = 1.2s \Rightarrow \theta = \frac{\Delta T}{\left(L_{mp}/a\right)} = 1.2 \qquad (6)$$

$$\Delta P = 220 - 70 = 150m \Rightarrow \Delta\eta = \frac{\Delta P}{(a.\Delta V / g)} = 0.712 \quad (7)$$

Step-4: Putting Θ calculated in step -3 to find UB location δ using equation (4)

$$\delta = \frac{2-\theta}{2} = 0.4 \Rightarrow X_p = 0.4 \times 1000 = 400m$$

Putting Δη calculated in step -3 to find UB diameter d* using equation (5)

$$d^* = \frac{\Delta\eta + 0.1747}{1.4157} = 0.6263 \qquad \Rightarrow D_{ub} = 0.6263 \times 0.3 = 188mm$$

Thus, the predicted values of X_p and D_2 are 400m and 188mm, as compared to the actual values of 400m and 180mm, respectively. This test confirms that the developed equations (equation 4 and 5) can be used for accurate prediction of UB location and size.

6.2 Limitation of the methodology

1. The current methodology is only for a single pipeline with single UB in it.
2. Steady state friction is used in the present study. However, unsteady friction inside the pipes may produce a different signal.
3. The present results are based on numerical modelling. Further validation is necessary against experimental results.
4. The signals may be influenced due to other fittings in the pipeline.

7. CONCLUSIONS

Following important conclusions are based on the present numerical study:

1. Pressure signals due to transients indicate presence of unauthorized branching (UB) in a pipeline.
2. The timing of a pressure drop can be used to predict UB location.
3. Pressure drop in the pressure signal can be used to predict UB size.

8. REFERENCES

Almeida, A. B. and Koelle, E., (1992), Fluid Transients in Pipe Networks, Computational Mechanics Publications, Elsevier, New York Beck, S. B. M.; Curren, M. D.; Sims, N. D.; and R. Stanway(2005), "Pipeline Network Features and Leak detection by Cross-Correlation Analysis of Reflected Waves," J. Hydraul. Eng., 131(8), 715–723

Chaudhry, M. H. (1987). Applied hydraulic transients. Van Nostrand Reinhold, New York, N.Y.

Liggett, J. A., and Chen, L.-C. (1994). "Inverse transient analysis in pipe networks." J. Hydraul. Eng., 120(8), 934–955.

Lighthill, J. (2001). Waves in fluids, Cambridge University Press, Cam- Bridge, U.K Wylie, E. B., Streeter, V. L., and Suo, Lisheng, (1993), Fluid Transient in Systems, Prentice-Hall, Englewood Cliffs.

Prediction Of Training Wall Height For Convergent Stepped Spillway - A Model Study

P. J. Wadhai[1], A. D. Ghare[2,] N. V. Deshpande[3]

[1] *Associate Professor, Department of Civil Engineering, G. H. Raisoni College of Engineering, C.R.P.F. Gate No. 3, Hingna Road, Digdoh Hills, Nagpur - 440 016, Maharashtra, India.,*
Email: prafull.wadhai@yahoo.com
Mobile No.: +91 9881 713 113

[2] *Associate Professor, Department of Civil Engineering, Visvesvaraya National Institute of Technology, Nagpur - 440 010, Maharashtra, India,*
Email: adghare@yahoo.co.in
Mobile No.: +91 9096 475 353

[3]*Principal, Guru Nanak Institute of Engineering & Technology, Kalmeshwar Road, Dahegaon, Nagpur - 441 501, Maharashtra, India,*
Email: narendravdeshpande@gmail.com
Mobile No.: +91 9960 180 795

A B S T R A C T

Enough interest has been generated worldwide amongst hydraulic researchers and engineers for the construction of stepped chutes. Increase in energy dissipation of flow over the spillway and ease of construction due to roller Compacted Concrete R.C.C.itself, are the basic reasons for its worldwide popularity. Sufficient number of literature references is available for the stepped chute design with straight side walls. On the other hand, a few literature references are available on the analysis and design of stepped spillways provided with convergent training walls on both sides. This paper presents the experimental investigations carried out on a spillway experimental set up having 0.7H:1V slope of stepped chute and training wall with 45° convergence. The variation in step height is accounted for, in the proposed graphs and expressions. The proposed expressions can be used for prediction of requirement of the training wall height and also for assessment of flow bulking, in stepped spillways with convergent training wall.

Keywords: Step height ratio, stepped spillways, convergence angle.

1. INTRODUCTION

A conventional ogee spillway profileprovided with series of steps from just below the crest up to the toe of the spillway has been represented as stepped spillway. The provision of series of steps on downstream face of the spillway chute significantly enhances the energy dissipation rate and reduces the size of energy dissipater which ultimately decreases the construction cost of stilling basin downstream of the spillway. Figure 1 shows the indicative cross section of stepped spillway.

Occurrence of high amount of air entrainment and lower flow velocities are mainly responsible for decrease in risk of cavitation resulting from excessive sub-pressures. Aeration produces bulking of flow and hence the spillway requires taller side walls. The effect of convergence increases this effect due to shock waves and higher training walls are required. Literature survey reveals that very few literature references is available on stepped spillways with convergent training walls in comparison with literature references available for stepped spillways with straight training walls. Due to limited scope for right-of-way caused by urbanization and because of the topographical or geological constraints, many ofthe stepped spillways are expected to be made with convergent training walls in due course of time. In the present experimental study, it is proposed to analyze the effect of convergence on flow characteristics of stepped spillway.

1.1 Indicativecross section of stepped spillway

D = Point of tangency

E = Toe of spillway

h = Normal size step height

h_1 = Flow depth measured vertically above the extreme corner of each step along the training wall

h_{1max} = Maximum flow depth measured vertically above the extreme corner of step along the training wall

H = Total drop height

H_d = Head over crest of spillway

H^1 = Drop height up to tangent point

l = Length of step

O = Crest of spillway

S = Distance measured from crest of spillway along the chute slope at extreme corner of step

S* = S / S_{max} = Dimensionless head at location of generation of h_{1max} S_{max} = Maximum distance measured from crest of spillway along the chute slope up to toe of spillway Y = Minimum depth of flow near the toe

Y_2 = Depth of flow after hydraulic jump

Z = Head measured vertically upward from toe of spillway

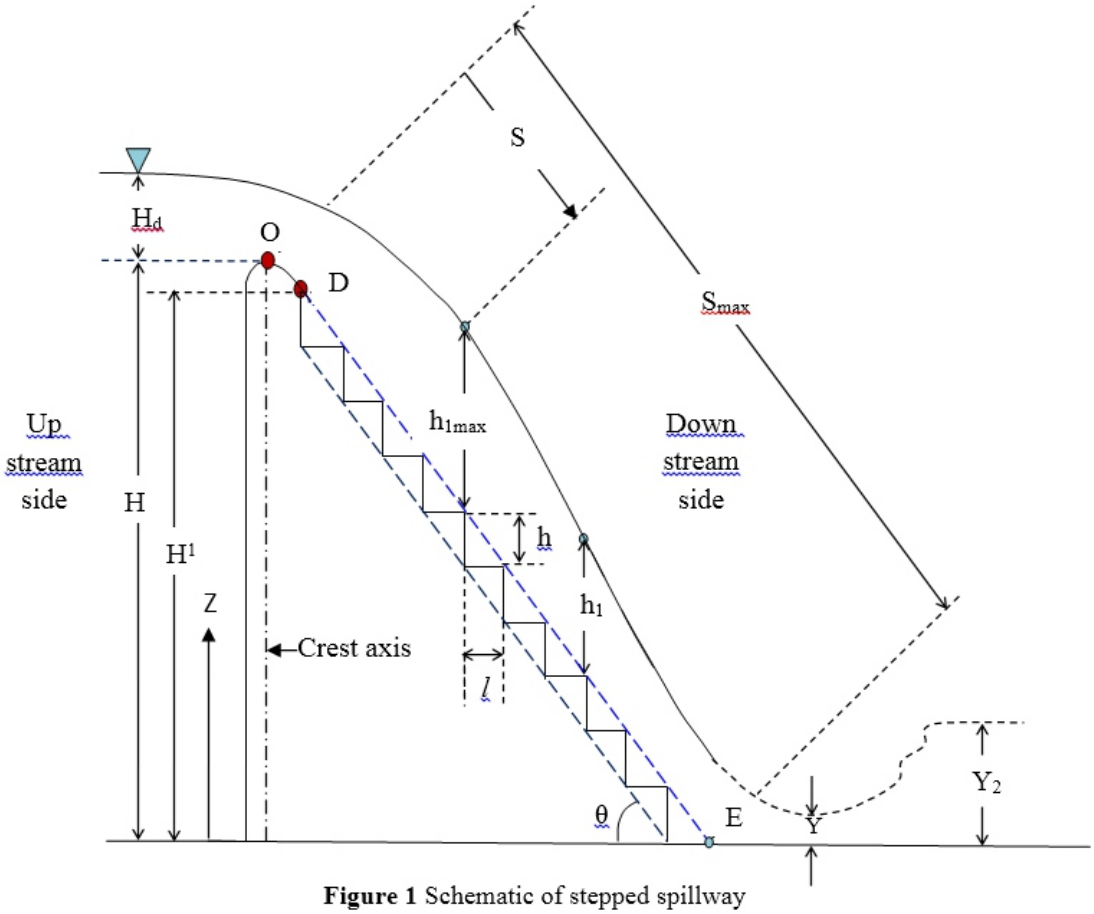

Figure 1 Schematic of stepped spillway

1.2 Literature review

Researchers viz. Sorensen (1985);Peyras et al. (1992); Christodoulou (1993); Chanson (1994);Chamani and Rajaratnam (1999);Barani et al. (2005); Chanson (2006);Chinnarasri and Wongwises (2006)and others highlighted the issues on study of stepped spillways. Hunt et al. (2008) performed experimental study on 1:22 scale three-dimensional, physical model. They analyzed the characteristics of flow over a sloping stepped chute (3H: 1V) in conjunction with varying angles of training wall. He observed that the height of training wall required, varied from critical depth of flow for convergence angle of 15° to three times the critical depth of flow for convergence angle 52°. Hunt et al. (2012), on the basis of simplified control volume momentum analysis and as a part of follow up work to their previous experimental study presented simplified generalized expression to estimate the vertical training wall height as a function of centerline flow depth. However, due to association of the force term during the derivation of the expression proposed, more testing and requirement of an empirical adjustment of this expression was warranted.With this background, it was felt necessary to conduct the experimental study to develop an expression to predict the training wall height for 45° convergent stepped spillways.Wadhai et al. (2014) performed experimental study over 1H:1V sloping stepped

chute with 45 degree convergence angle normalized by different step height ratio. Author proposed the regression equation for training wall height of convergent stepped spillway.In order to estimate the surface roughness length z_0, displacement height *ds* and the relationship of *ds* and $z_{0,}$ an exhaustive analysis was performed by Cheng et al. (2014). He expanded the available data from step geometry and summarized that, *ds* and z_0 depended on a key factor i.e. hydraulic roughness height *k*s..

2. EXPERIMENTAL PROGRAM

Water was liftedfrom existing underground sump by means of water recirculation system aligned with a centrifugal pump of 10 HP capacity and dischargedthrough delivery pipe in to upstream storage reservoir of 15750litres capacity. The delivery pipe equipped with venturimeterand U-tube manometer for measurement of flow rate. The storage reservoir was followed by ogee type 2.02 m wide long crested weir and 0.7(H):1(V) slope (i.e. $\theta = 55^o$)stepped chute and a toe channel of 0.5 m wide and 10 meter long.Side walls of the stepped spillway had a convergence angle of $Ø = 45^o$ fromboth sides. The training walls of convergent stepped spillway and side walls of toe channel were fabricated with acrylic sheet for clear visibility of flow over the stepped spillway and in toe channel. Discharge measuring devices viz. venturimeterand a triangular notch were calibrated prior to the experimentation.

Normal size step heights of (h) =0.12 m, 0.06 m, 0.03 m and 0.015 m were tested during the experimental study which corresponded to equivalent step height ratios, $H^* = (H^1/ h)$ of 10, 20, 40 and 80 respectively. Water from upstream storage reservoir was allowed to pass over the convergent stepped spillway of total drop height H = 1.26 m and subsequently flowedthrough a toe channel and discharged into a collecting tank for measurement of discharge. Discharge was measured in a normal range of 0.022cumec to 0.065cumec.Vernier type point gauges were used with a sensitivity of 0.1 mm for measurement of water levels in horizontal and vertical directions on the step and also for measurement of flow depths at other locations.

Convergent stepped spillway experimental model constructed at G. H. Raisoni College of Engineering, Nagpur in collaboration with VNIT, Nagpur, Maharashtra State, India used in this study is shown in Figure 2.

Figure 2 Photograph showing experimental setup during a run

3. EXPERIMENTAL DATA AND COMPUTATIONS

Table 1, Table 2, Table 3, Table 4 and Table 5 present the data sets of observations and the required computations for the different experimental runs for the various step height ratios (H*) and also for smooth ogee spillway. These tables also show the observed maximum depth of flow along the converging training walls in dimensionless form and the corresponding flow regime for the different experimental runs.

Table 1 Experimental data and computations for θ = 55º, Ø = 45º, H* = 10, L = 2.02 m and h = 0.12 m

Intensity of discharge at crest of spillway	Critical depth of flow	Total Drop Height	Dimensionless Discharge	Dimensionless maximum depth of flow along the side wall	Flow Regime
$q = Q/L$	$Y_c = (q^2/g)^{1/3}$	H	$Q/(H_d^{5/2} * g^{1/2})$	h_{1max}/h	—
m^2/s	m	m	—	—	—
0.0101	0.0218	1.26	51.41	0.9292	Nappe
0.0157	0.0293	1.26	38.24	1.1117	Nappe
0.0217	0.0363	1.26	30.84	1.2758	Partly skimming
0.0276	0.0427	1.26	26.28	1.3875	Partly skimming

Table 2 Experimental data and computations for θ = 55°, Ø = 45°, H* = 20, L = 2.02 m and h = 0.06 m

Intensity of discharge at crest of spillway	Critical depth of flow	Total Drop Height	Dimensionless Discharge	Dimensionless maximum depth of flow along the side wall	Flow Regime
$q = Q/L$	$Y_c = (q^2/g)^{1/3}$	H	$Q/(H_d^{5/2} * g^{1/2})$	h_{1max}/h	—
m^2/s	m	m	—	—	—
0.0123	0.0249	1.26	45.04	2.1600	Partly skimming
0.0159	0.0296	1.26	37.94	2.4450	Partly skimming
0.0200	0.0344	1.26	32.62	2.7567	Partly skimming
0.0253	0.0402	1.26	27.88	3.0867	Skimming
0.0295	0.0446	1.26	25.11	3.3583	Skimming

Table 3 Experimental data and computations for θ = 55°, Ø = 45°, H* = 40, L = 2.02 m and h = 0.03 m

Intensity of discharge at crest of spillway	Critical depth of flow	Total Drop Height	Dimensionless Discharge	Dimensionless maximum depth of flow along the side wall	Flow Regime
$q = Q/L$	$Y_c = (q^2/g)^{1/3}$	H	$Q/(H_d^{5/2} * g^{1/2})$	h_{1max}/h	—
m^2/s	m	m	—	—	—
0.0119	0.0244	1.26	45.92	3.7533	Skimming
0.0173	0.0313	1.26	35.83	4.5267	Skimming
0.0208	0.0353	1.26	31.74	5.0167	Skimming
0.0259	0.0409	1.26	27.44	5.7033	Skimming
0.0312	0.0463	1.26	24.21	6.3967	Skimming

Table 4 Experimental data and computations for θ = 55°, Ø = 45°, H* = 80, L = 2.02 m and h = 0.015 m

Intensity of discharge at crest of spillway	Critical depth of flow	Total Drop Height	Dimensionless Discharge	Dimensionless maximum depth of flow along the side wall	Flow Regime
$q = Q/L$	$Y_c = (q^2/g)^{1/3}$	H	$Q/(H_d^{5/2} * g^{1/2})$	h_{1max}/h	—
m^2/s	m	m	—	—	—
0.0124	0.0250	1.26	44.76	5.7933	Skimming
0.0166	0.0303	1.26	36.95	7.0067	Skimming
0.0201	0.0345	1.26	32.47	7.9400	Skimming
0.0253	0.0402	1.26	27.88	9.2133	Skimming
0.0317	0.0468	1.26	23.97	10.7067	Skimming

Table 5 Experimental data and computations for θ = 55°, Ø = 45°, smooth ogee chute and L = 2.02 m

Intensity of discharge at crest of spillway	Critical depth of flow	Total Drop Height	Dimensionless Discharge	Dimensionless maximum depth of flow along the side wall	Flow Regime
$q = Q/L$	$Y_c = (q^2/g)^{1/3}$	H	$Q/(H_d^{5/2} * g^{1/2})$	h_{1max}/h	—
m^2/s	m	m	—	—	—
0.0127	0.0254	1.26	44.06	—	Skimming
0.0175	0.0315	1.26	35.56	—	Skimming
0.0208	0.0353	1.26	31.74	—	Skimming
0.0256	0.0406	1.26	27.60	—	Skimming
0.0313	0.0464	1.26	24.17	—	Skimming

4. ANALYSIS OF EXPERIMENTAL DATA

The required training wall height is governed by the flow run- up due to convergence of the chute walls. For any of the step height ratios it was visualized that there were no transverse waves on the other hand it was observed that the air entrainment occurred for nearly all the observations. Water surface profiles has been plotted along the centerline of the spillway and also along the convergent side walls from the data collected during the experimental study. As anticipated, the flow depths observed near the wall were more than those observed at the centerline of the spillway. The flow depths along sidewall shall form the basis for prediction of requirement of minimum height of training wall so that the flow does not overtop the convergent side walls and maintaining the safety of the structure.

4.1 Graphical representation

Figure 3 (a), (b), (c), (d) and (e)showthe water surface profiles observed along the wall for different discharges for a step height ratio $H^* = (H^1/h) = 40$.

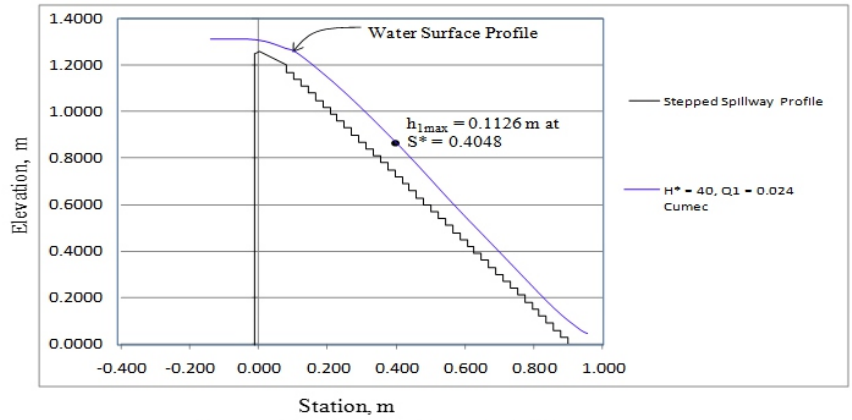

Figure 3 (a) Water surface profiles along the side wall of spillway for θ = 55°, Ø = 45° and step height ratio H* = 40, Q_1 = 0.024 cumec

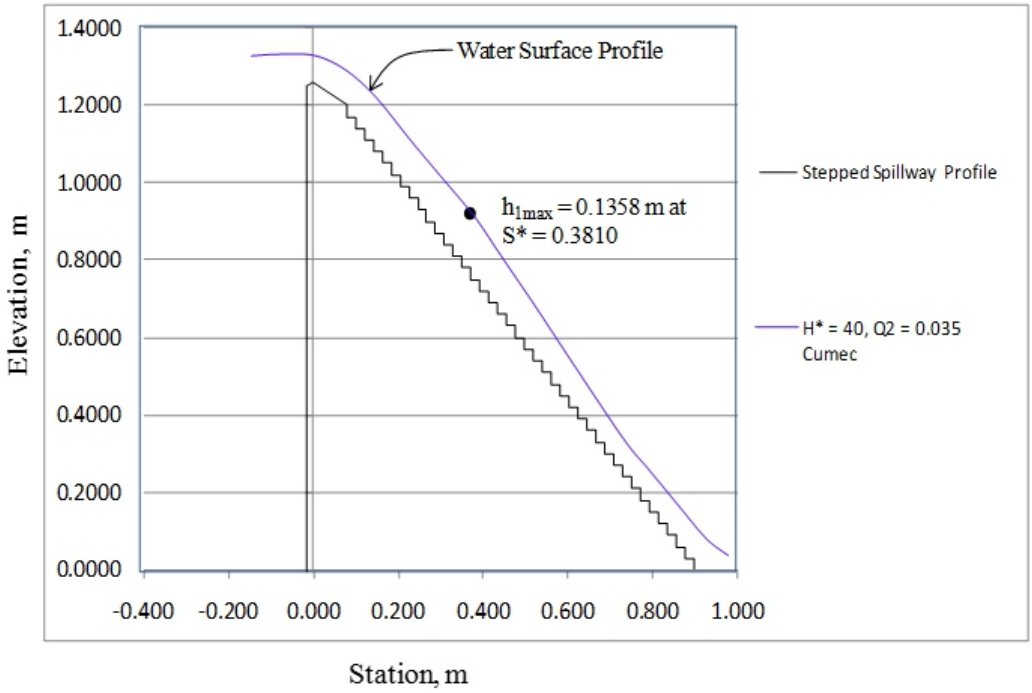

Figure 3 (b) Water surface profiles along the side wall of spillway for θ = 55°, Ø = 45° and step height ratio H* = 40, Q_2 = 0.035 cumec

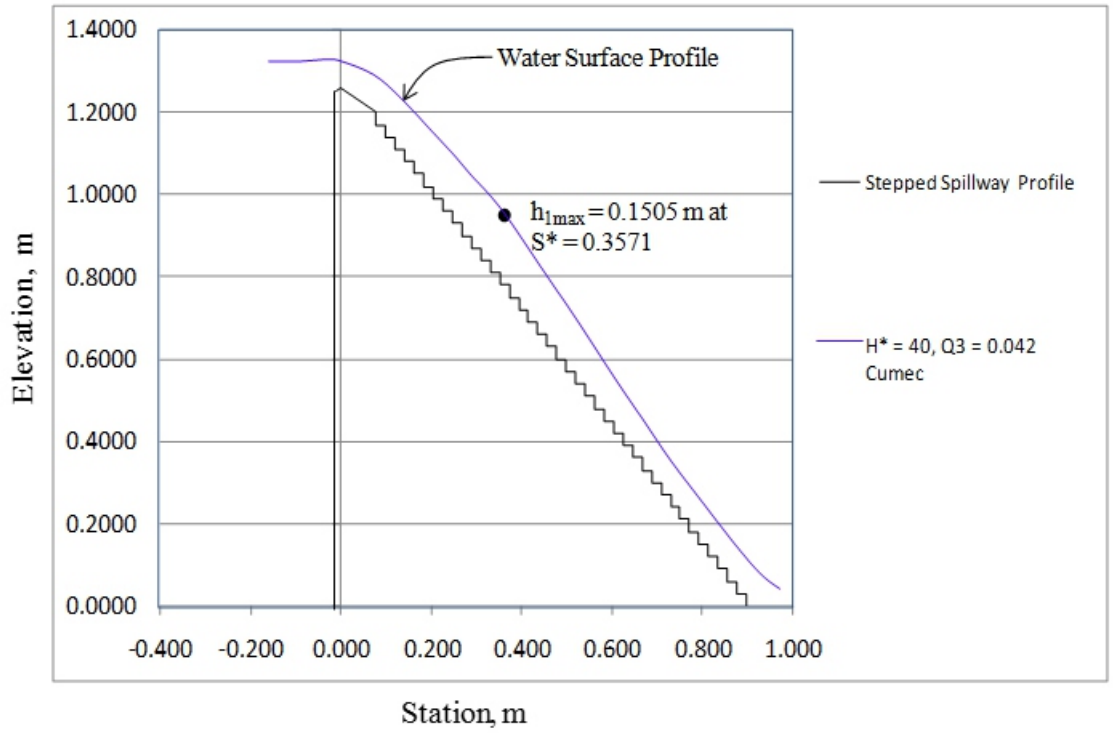

Figure 3 (c) Water surface profiles along the side wall of spillway for θ = 55°, Ø = 45° and step height ratio H* = 40, Q_3 = 0.042 cumec

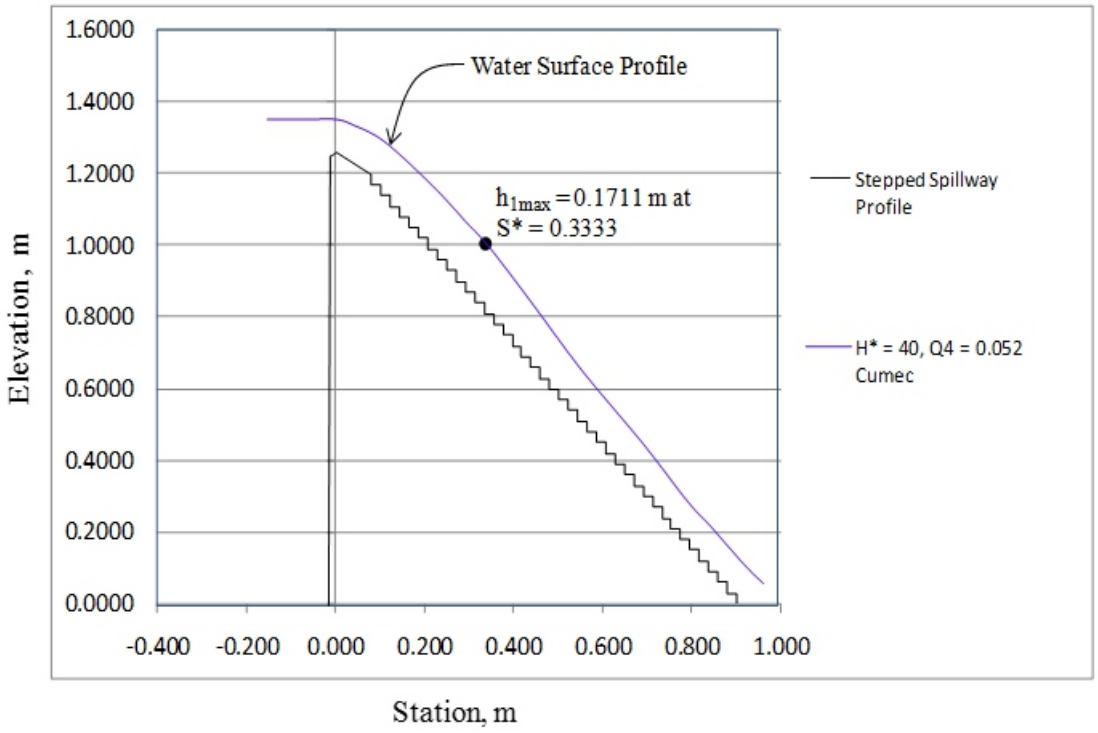

Figure 3 (d) Water surface profiles along the side wall of spillway for θ = 55°, Ø = 45° and step height ratio H* = 40, Q_4 = 0.052 cumec

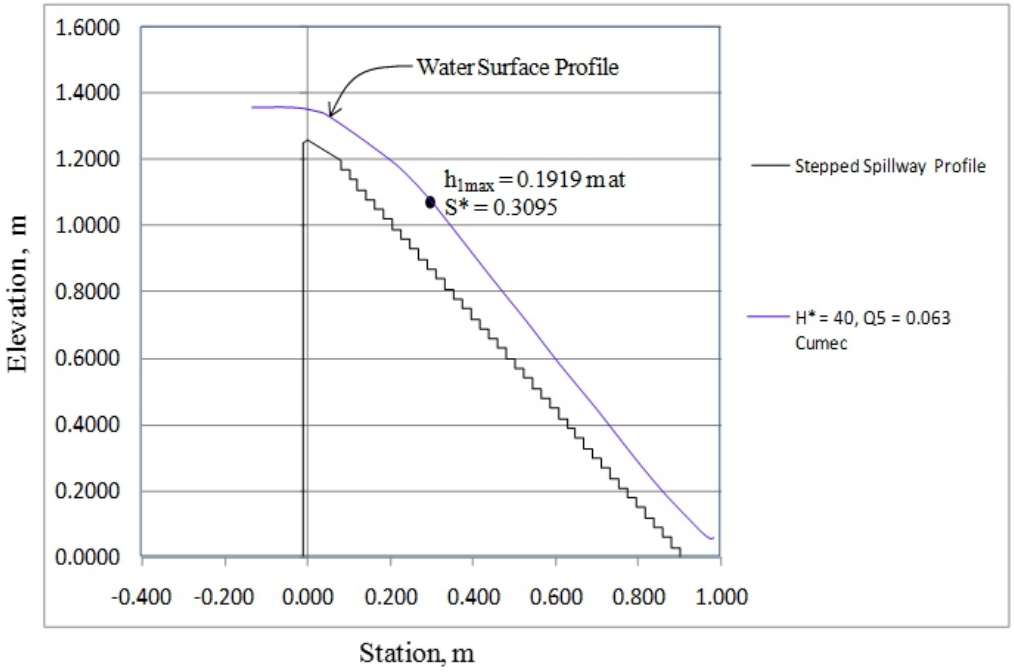

Figure 3 (e) Water surface profiles along the side wall of spillway for θ = 55°, Ø = 45° and step height ratio H* = 40, Q_5 = 0.063 cumec

As the maximum flow depth along the wall (h_{1max}) would determine the requirement of training wall height, a plot showing its variation with discharge in dimensionless form is presented in Figure (4).

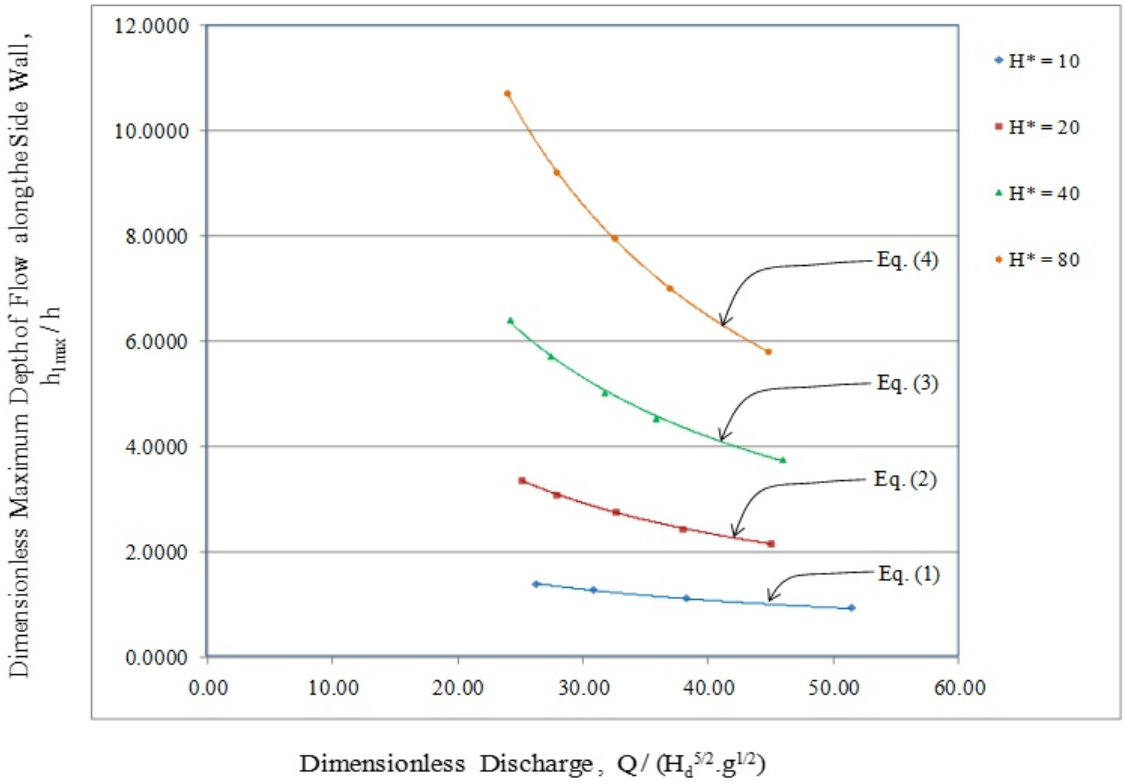

Figure 4 Dimensionless maximum depth of flow along the side wall versus dimensionless discharge for θ = 55°, Ø = 45° and step height ratio H*= 10, 20, 30 and 40

4.2 Regression equations

From a plot showing variation of observed dimensionless maximum depth of flow along the side wall versus dimensionless discharge for θ = 55° and ø = 45° as presented in Figure (4), the regression equations have been obtained and are as follows.

$$For H^* = 10,\ \left[\frac{h_{1max}}{h}\right] = 10.02\left[\frac{Q}{\left(H_d^{5/2}.g^{1/2}\right)}\right]^{-0.60},\ R^2 = 0.999 \quad (1)$$

$$For H^* = 20,\ \left[\frac{h_{1max}}{h}\right] = 38.17\left[\frac{Q}{\left(H_d^{5/2}.g^{1/2}\right)}\right]^{-0.75},\ R^2 = 0.999 \quad (2)$$

$$For H^* = 40,\ \left[\frac{h_{1max}}{h}\right] = 90.29\left[\frac{Q}{\left(H_d^{5/2}.g^{1/2}\right)}\right]^{-0.83},\ R^2 = 0.998 \quad (3)$$

$$For H^* = 80,\ \left[\frac{h_{1max}}{h}\right] = 241.6\left[\frac{Q}{\left(H_d^{5/2}.g^{1/2}\right)}\right]^{-0.98},\ R^2 = 1.000 \quad (4)$$

These expressions are proposed to be used for computation of training wall height of convergent stepped spillway only with convergence angle of 45° and chute slope of 0.7H:1V.

Table 6 summarizes the comparison of observed maximum depth of flow along side wall (h_{1max}) with the corresponding critical depths of flow (Y_c).

Table 6 Comparison of observed maximum depth of flow along side wall (h_{1max}) with corresponding critical depths of flow (Y_c) for θ = 55°, Ø = 45°, smooth ogee chute and L = 2.02 m

Flow Run up	Step height ratio	Step height	Observed maximum depth of flow along the converging training wall
—	$H^* = (H^1/h)$	h	h_{1max}
—	—	m	m
1	10	0.12	$3.90Y_c$ to $5.11Y_c$
2	20	0.06	$4.51Y_c$to $5.21Y_c$
3	40	0.03	$4.14Y_c$ to $4.61Y_c$
4	80	0.015	$3.43Y_c$ to $3.47Y_c$
5	Smooth ogee	Smooth ogee	$3.43Y_c$ to $3.46Y_c$

5. CONCLUSIONS

An experimental study has been carried on convergent stepped spillway having 0.7H:1V chute slope and 45° convergence angle for different step height ratios. The flow over the convergent stepped spillway was observed to be more bulked and air entrained as compared to ogee spillway. Stepped spillways with convergent training walls may have to be employed for spillway rehabilitation work with inadequate availability of downstream space. Only a few guidelines are available in the literature for design of convergent stepped spillways.

It was observed that, as the dimensionless discharge increases, the maximum flow depth at the convergent training wall decreases. The regression equations {Eq. (1) to (4)} for prediction of maximum depth of flow near the converging walls have been proposed on the basis of experimental observations and analysis for different step height ratios. A good correlation was obtained for all the regression equations indicating high value of determination coefficient. In general, the maximum depth of flow near the convergent training wall was found to lie between 3.43 to 5.21 times of the critical depth of flow, on the basis of different step height ratios. The regression equations presented in this paper, may be useful for the hydraulic design engineers associated in estimation for deciding the appropriate height of training wall for convergent stepped spillways. However, more experimental studies with different convergence angles shall be required, to formulate more generalized expressions for estimation of

of adequate training wall heights for convergent stepped spillways.

ACKNOWLEDGEMENTS

The research presented in this paper is based on a research project funded by Raisoni Group of Institutions (RGI), India, which is gratefully acknowledged by the authors.

Notations

The following symbols are used in this paper :

A = $L * H_d$ = Area of flow at crest of spillway;
A_1 = $B * Y$ = Area of flow at toe of spillway;
B = Width of flow channel;
C = Discharge coefficient;
E_r = $\Delta E / E_o$ = Relative energy dissipation;
E_o = $H + 1.5\ Y_c$ = Energy at crest of spillway;
E_t = $Y + (V_1^2 / 2.g)$ = Energy at toe of spillway;
g = Acceleration due to gravity;
h = Normal size step height;
h_{1max} = Maximum depth of flow observed along the converging training wall;
h_1 = Depth of flow observed along the converging training wall;
H = Datum head measured from toe up to crest of Spillway;
H_d = Head over crest of spillway;
H^1 = Drop height;
H^* = H' / h = Step height ratio;
L = Length of crest;
Lr = Lp / Lm = Scale ratio;
n = Number of regular size steps;
q = Q / L = Intensity of Discharge;
Q = $C * L * (H_d)^{1.5}$ = Rate of flow i.e. Discharge over crest of spillway;
R = Hydraulic radius;
V = Q / A = Velocity of flow at crest of spillway;
V_1 = Q / A_1 = Velocity of flow;
Y = Depth of flow;
Y_c = Critical depth of flow;
ΔE = $E_o - E_t$ = Energy loss due to stepped spillway;
$\emptyset$ = Convergence angle;
θ = Chute angle;

REFERENCES

Sorensen, R. M. (1985).Stepped spillway hydraulic model investigation.J. of Hydraul Eng., 111(12), 1461 - 1472.
Peyras, L., Royet, P. and Degoutte, G. (1992). Flow and energy dissipation over stepped gabion weirs.J. of Hydraul Eng., 118(5), 707-717.
Christodoulou, G. C. (1993). "Energy dissipation on stepped spillways."J. of Hydraul Eng., 119(5), 644 - 649.
Chanson, H. (1994).Hydraulics of skimming flow over stepped channels and spillways. J. of HydraulRes., 32(3), 445 - 460.
Chanson, H. (1994 a).Comparison of energy dissipation between nappe and skimming flow regime on stepped chutes.J. of Hydraul Eng., Res., IAIHR, 32(2), 213 - 218.
Chamani, M. R. and Rajaratnam, N. (1999).Characteristics of skimming flow over stepped spillways.J. of Hydraul Eng., 125(4), 361 - 368.
Barani, G. A., Rahnama M. B. and Sohrabipoor, N. (2005).Investigation of flow energy dissipation over different stepped spillways.American Journal of Applied Sciences., ISSN 1546-9239, 2 (6), 1101- 1105.

Chanson, H. (2006).Hydraulics of skimming flow on stepped chutes : The effects of inflow conditions." J. of Hydraul, Res., 44(1), 51 - 60.

Chinnarasri, C. and Wongwises, S. (2006). Flow pattern and energy dissipation over various stepped chutes. J. of Irrig. Drain. Eng., 132 (1), 70 - 76.

Sherry L. Hunt, Kem C. Kadavy, Steven R., and Darrel M. Temple (2008). Impact of converging chute walls for roller compacted concrete stepped spillways. J. of Hydraul Eng., ASCE, 134 (7), 1000 - 1003.

Sherry L. Hunt, Darrel M. Temple, Steven R., Kem C. Kadavy, and Greg Hanson. (2012). Converging stepped spillways: simplified momentum analysis approach. J. of Hydraul Eng., ASCE, 138 (9), 796 - 802.

Wadhai, P. J., Deshpande, N. V. and Ghare, A. D. (2014).Experimental investigations for estimation of the height of training wall of convergent stepped spillways.International Journal of Engineering Research [IJER], IJER ISSN : 2319 - 6890 (Online), 2347 - 5013 (Print), Volume 3 (Special Issue 3), Page 23 - 27, 18 - 20, December 2014.

Cheng, X., Gulliver, J. S. and Zhul, D. (2014).Application of displacement height and surface roughness length to determination boundary layer development length over stepped spillway. ISSN 2073 - 4441, Water2014 (6), 3888 - 3912.

Determination Of Residual Energy For Flow Over Trapezoidal Labyrinth Weir

Dr. Bhalchandra V. Khode
Professor, Civil Engineering Department, G.H.Raisoni College of Engineering, Nagpur.
Email:- bhalchandra.khode@raisoni.net

A B S T R A C T

The capacity of an existing spillway can be increased by lengthening the spillway crest, or increasing the discharge coefficient or the operating head, or any combination of these approaches. This type of weir is more economical and effective solution to increase the discharge by increasing the spillway crest length without an associated increase in structure width. Use of labyrinth spillway is particularly suited to sites where the spillway width and upstream water surface are limited and larger discharging capacities are required. Constructing a labyrinth weir in an existing spillway is an example of an effective way to increases the spillway crest length and the corresponding discharge capacity for the same operating head. This type spillway may also provide additional reservoir storage capacity as compared to more costly gated spillway, while comparing the original spillway discharge. The present research mainly aims at evaluating the relative residual energy at the base of labyrinth weir and vertical drops. The result show that relative energy at the toe of the labyrinth weir is smaller than that of vertical drops due to total upstream head and the length magnification(L/W). This paper deals with outcome of the experiments to study difference between the relative residual energy at the toe of the labyrinth weir and vertical drops for wider practical range of side wall angles (α) from 6˚ to 30˚ and length magnification (L/W= 4.23 to1.25).

Keywords: Labyrinth weir, Length magnification (L/W) ,Residual energy

1. INTRODUCTION

Labyrinth weir have the distinguish characteristics of a relatively high discharge for a given head, relative to linear weir of the same width (Fig.1). Labyrinth spillway can be economical solution for increasing unit discharge over conventional weirs for a given head. Particularly suited for use as a service or emergency spillway at a reservoir site where large discharge is to be handled at relative narrower waterway. An extensive investigation on the influence of geometric and hydraulic parameters on the hydraulic behavior of labyrinth weirs, particularly on the discharge capacity, has been done by several researchers. Taylor (1968) extensively studied the behavior of labyrinth weir and presented the hydraulic performance as it compares to that of sharp-crested weir. Hay and Taylor (1970) followed up on Taylor's work and developed design criteria for labyrinth weirs. Additional work by Darvas (1971)

utilized the results from physical model studies to expand on the theory and developed a family of curves to evaluate spillway performance. Extensive physical model studies were performed by Houston (1983) to evaluate various labyrinth geometries and approach conditions. U.S. Bureau of Reclamation (USBR) tested model of labyrinth spillway for Ute Dam and Hyrum Dam (Houston 1983, 1984). They found that the discrepancy between their result and those of Hay and Taylor (1970) were due to difference in head definition. Megalhaes and Lorena (1985) developed curves similar to that of Darvas (1971) except their curves are for a nappe or ogee shaped crest. Lux (1984) studied the hydraulic performance of Labyrinth weirs using dimensional analysis and developed an equation for the discharge of the labyrinth weir from the data obtained from flume studies. Megalhaes (1989) introduced some modification to the Darvas approach by non-dimensionalising the discharge coefficient. However, the discharge coefficient design charts developed by Megalhaes do not match the results of Darvas for a similar shape of spillway. Megalhaes and Lorena (1989) developed curves for a dimensionless discharge coefficient on the relative total upstream head , in the magnification ratio or on the angle side legs, on aeration effects, on weir shape and flow condition in the approach and down channels. Tullis et al. (1995) carried out extensive experimental work on performance of the labyrinth weir and presented Discharge coefficient curves in simplified way as compared to previous investigators. They proposed a method for designing a labyrinth weir by using the basic equation used for linear weir which would also be applicable to labyrinth weir with modification in coefficient of discharge. Tullis et al. (2005) also conducted test to optimize the performance of 7˚ & 8˚ labyrinth weirs at low heads for different crest shape. Further, Tullis et.al (2007) conducted experiments to find effect of submerged condition and developed head-discharge relationship. Khode et.al (2012) carried out experimental studies on flow over labyrinth weir using four models of side wall angles 6˚,8˚,20˚ and30˚ keeping the height of trapezoidal labyrinth weir constant at P=0.10 and P=0.075m. There is also limited knowledge on the relative residual energy at the base of the labyrinth. In the present paper an experiment are conducts to determine relative residual energy at the base of the vertical drops for range of 6˚ 8˚ 10˚ 20˚and 30˚. Design curves are obtained from the experimentation data and relation between residual energy at the toe of the labyrinth weir and vertical drops and the dimensionless parameters (Ht/P) is presented.

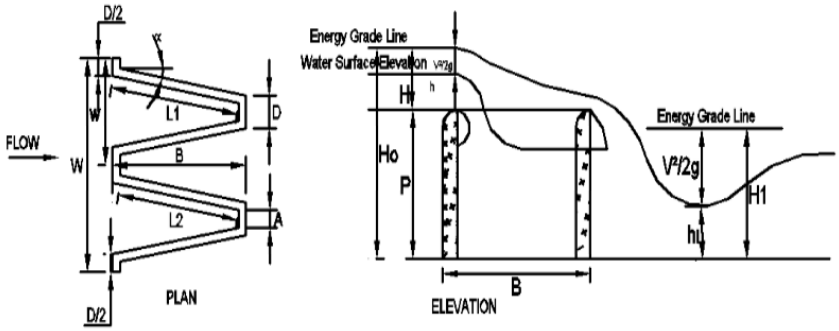

Fig.1Layout and Details of Labyrinth weir

2. MATHEMATICAL FORMULATION FOR LABYRINTH WEIR

A labyrinth spillway is an overflow weir folded in plan view to provide a longer total effective length for a given overall spillway width (Fig.-1). It is relatively slender walls having a respective plan form, shaped generally triangular or trapezoidal, with a vertical upstream face. The flow over labyrinth weir is three dimensional and does not readily fit into mathematical description and hence the discharge function is found through experimental studies and analysis. The capacity of labyrinth weir is a function of total head, the effective crest length and the Discharge coefficient. The Discharge measured with triangular notch placed upstream from the weir channel region. Three point gauges were used to measure water levels in the flume.

1) The discharge per unit width of weir can be expressed as $q = \frac{Qm}{W}$ ------(1)

Where,

Q_m= Discharge over labyrinth weir,

W= Width of labyrinth weir.

2) Critical depth of flow $Y_C = \left(\frac{q^2}{g}\right)^{1/3}$ ----------(2)

3) Energy at the crest of the spillway $H_O = P + 1.5Yc$ ---------(3)

4) Velocity of flow $V = \frac{Qm}{B \times Y}$ ---------(4)

5) Energy at the toe of the spillway $Et = y + \frac{V^2}{2g}$ --------(5)

6) Energy loss due to labyrinth $H_1 = E - Et$ ---------(6)

7) Relative Energy loss $E_R = \frac{H_1}{H_O}$ ---------(7)

3. EXPERIMENTAL SETUP

The experimental set-up mainly consists of sump, pumping system, initial discharge tank, rectangular flume, discharge measuring unit and labyrinth weir. The schematic arrangement of the experimental set up is shown in Fig.2. The water used for experimentation was pumped from a sump (2.5x2.5x2.5m) through 10H.P pump and main pipe line of 150mm diameter into initial discharge tank of size 2.5 x 1.0x 0.65.m having triangular notch on one side to measure initial discharge. A precisions point gauge was used to determine the elevation of the weir crest and obtained the water surface elevation of approaching flow. The point gauge had a vernier scale that was marked in 0.1mm increments. The kinetic energy of the flow is reduced by a steel grate with many 3/16-inch diameter holes was placed across the head of the flume. Further reduction in splashing was done by keeping wooden grate floating to obtain more uniform water surface entering the experimentation flume. The inflow was regulated to the desired flow by operating the valve. The water is then allow to 0.5m wide x 0.5m deep x 3.4m long rectangular flume having an arrangement to place various labyrinth weir of different geometries. A traversing point gauge

having accuracy of 1mm was mounted on roller carriage track running the length of the flume. To ensure correct piezometric head measurement and account for deviations in the correction factor was added to the point gauge reading which was predetermined by using a static water surface in the flume. The gauging station was located such that it avoids the area of water surface draw-down, yet closed enough for the energy loss between the gauging station and structure to be negligible. It was located between four to five times the maximum total head over the weir upstream from the face of the weir. The experimentation flume is mounted on steel super structure with jack assembly to control the slope. The dimensions of quarter round crest shape labyrinth weir having different geometrics based on varying side wall angle of 6º,8 º,10 º,20º & 30 º used during experimentation. Each labyrinth weir was approximately 0.15 m in height, fabricated using 15mm thick acrylic sheet material and having two complete labyrinth weir cycles. Each labyrinth weir was tested at a height P equal to 0.15m. All the weirs were installed at the position of the flume to provide an unrestricted supply of air under the nappe. Dimension of all the models are given in Table.1

Table .1 Geometrics for Labyrinth Weir Used in the Present Study

Side wall angle (α)	Height of Weir (P) (m)	Number of Cycles	Apex Width (A) (m)	Length of one cycle	Total crest length	Effective Crest Length $L=N(2L_2+2A)$ (m)	Length Magnification (L/W)
6°	0.15	2	0.03	0.690	1.579	1.271	4.23
8°	0.15	2	0.03	0.545	1.091	0.986	3.28
10°	0.15	2	0.03	0.458	0.917	0.816	2.72
20°	0.15	2	0.03	0.282	0.565	0.4814	1.60
30°	0.15	2	0.03	0.222	0.445	0.376	1.25

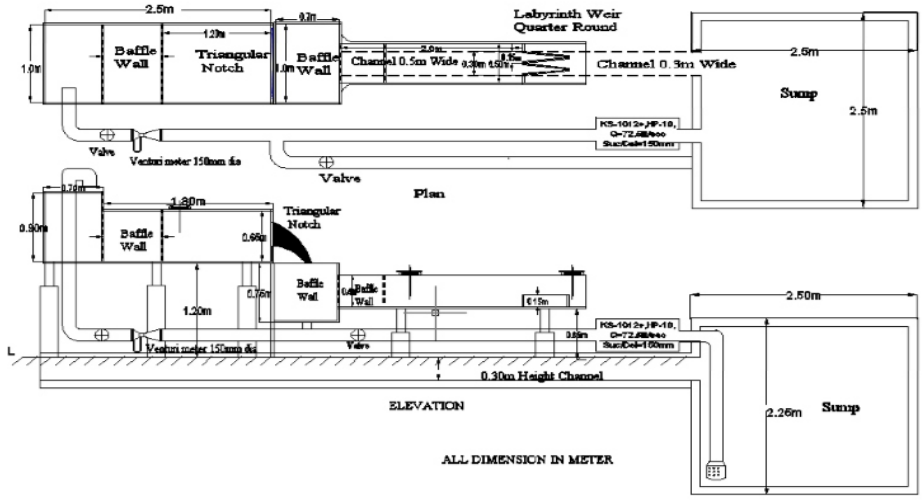

Fig.2 Schematic arrangement of Labyrinth weir

4. EXPERIMENTAL PROCEDURE

Each labyrinth weir was then tested with a starting inflow 0.005m3/s, which was gradually increased at each increment of flow so as to obtain increment of Ht/P ratio of 0.10. The testing was done for each weir for a range of flow to cover H/P ratio from 0.1 to 0.8. The flow rates were measured using calibrated triangular notch. The total head over the weir was taken as the difference in the water surface and the crest plus the velocity head and was measured at 4 to 5 times the maximum total head over the weir upstream from the face of the weir. For each test run, the flow in channels was allowed to become stable, and the flow rate readings were repeated to obtain accurate reading at steady conditions. The limiting condition and the ranges of variable covered in this study for Labyrinth weirs are shown as follows.

Length magnification =4.23 to 1.25

Side wall angle = 6^0, 8^0, 10^0,20^0 and 30^0

Vertical aspect ratio (w/P) =2.5

Height of weir (P) = 0.15m

Head to weir height (H/P) =0.15 to 0.8

5. RESULTS AND DISCUSSIONS

Experimentation are carried out on different quarter round trapezoidal labyrinth weir with side wall angle 6º to 30º. For each model of labyrinth weir the discharge is adjusted at different value in the range 0.005 m^3/sec to 0.018 m^3/sec and head is measured for each value of discharge as well as water levels upstream and downstream of the labyrinth weir. From these observations the value of total energy upstream of the labyrinth weir and residual energy at the base of the labyrinth weir is calculated based on equation (1to 7) and variation of H_1/H_0 with H/P is plotted in a graph as shown in Fig.1. To represent the data in the of equation form, regression analysis is carried out for the observed data for each model separately. It is found that logarithmic curve fits well to obtained relation between H_1/H_O and Ht/P therefore residual energy at the base of the labyrinth weir (H_1/H_O) is expressed.

$$\frac{H_1}{H_0} = 0.233ln\left(\frac{H}{P}\right) + 0.763 \quad R^2=0.995 \quad \text{for Length magnification } \frac{L}{W} = 4.23 \quad \text{-------(8)}$$

$$\frac{H_1}{H_0} = 0.247ln\left(\frac{H}{P}\right) + 0.703 \quad R^2=0.986 \quad \text{for Length magnification } \frac{L}{W} = 3.28 \quad \text{-------(9)}$$

$$\frac{H_1}{H_0} = 0.228ln\left(\frac{H}{P}\right) + 0.631 \quad R^2=0.988 \quad \text{for Length magnification } \frac{L}{W} = 2.72 \quad \text{-------(10)}$$

$$\frac{H_1}{H_0} = 0.237ln\left(\frac{H}{P}\right) + 0.595 \quad R^2=0.980 \quad \text{for Length magnification } \frac{L}{W} = 1.60 \quad \text{------ (11)}$$

$$\frac{H_1}{H_0} = 0.231ln\left(\frac{H}{P}\right) + 0.550 \quad R^2=0.972 \quad \text{for Length magnification } \frac{L}{W} = 1.25 \quad \text{----- (12)}$$

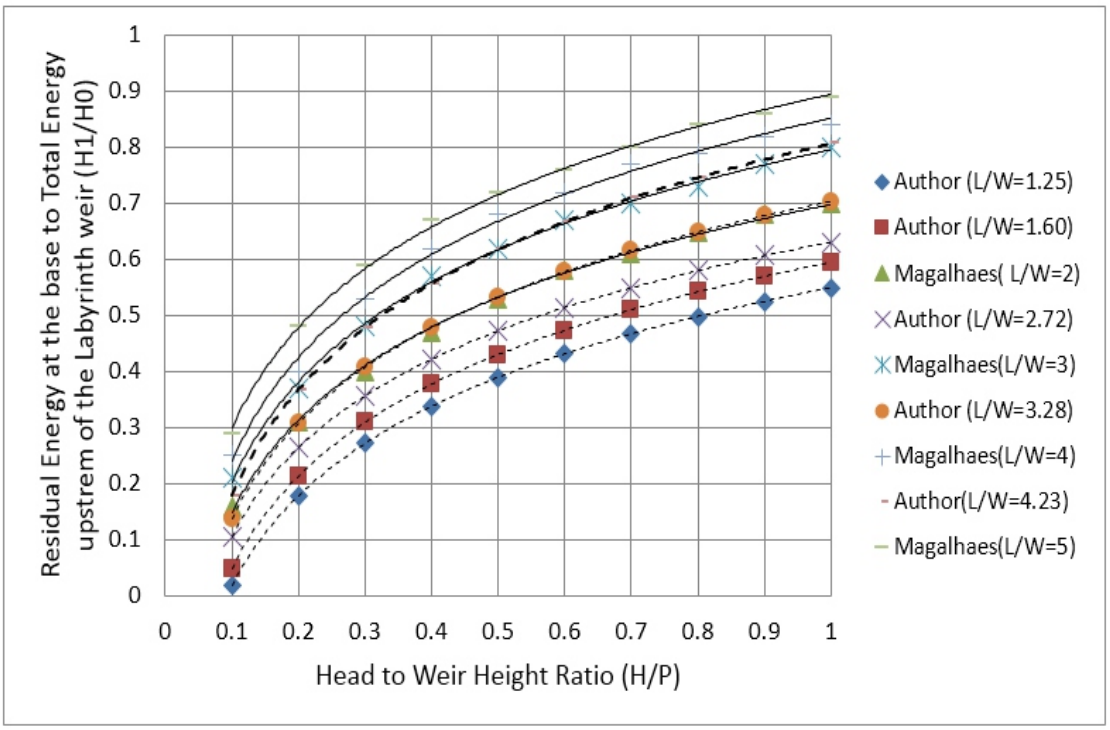

Fig.3 Comparison of Residual Energy at the base to total energy upstream of labyrinth weir and Estimated Residual Energy at the base to total energy upstream of labyrinth weir by Magalhaes and Lorena

7. CONCLUSION

Labyrinth weir is an economical flood discharging structure, particularly suited for use at sites where the head is limited or the spillway width is restricted by the topography. Compared with traditional gated spillway, a free-flow labyrinth is more reliable for increasing the flood discharge and storage capacity of existing dams. Based on experimental data obtained from flume studies on labyrinth weirs of side wall angles 6,8,10,20 and 30 degree and upstream quarter round crest on upstream face, the following conclusions are drawn.

1. The relative residual energy at the base of the labyrinth weir (H_1/H_O) is increase with the relative total upstream head (H/P).
2. The Relative energy maximum for maximum length magnification and decreases with decrease in length magnification.
3. The relative residual energy at the base of labyrinth weirs varies between 0.16 and 0.85, corresponding to energy loss .Hence the labyrinth weir highly effective in energy dissipation, particularly for small values of relative total upstream head (H/P).

NOTATION

The following symbols are used in this paper:

A = The length of the inside apex ;

D = Outside width of apex;

g = Gravitational acceleration constant;

H = Total upstream head over labyrinth weir;

Hd = design head;

Ho = total energy upstream of the labyrinth weir;

H1 = residual energy at the base of the labyrinth weir

h = Piezometric head over the weir;

y = flow depth at the base of the labyrinth weir.

q. = discharge per unit width.

N = number of labyrinth cycles

L_1 = length of side leg;

L_2 =Effective side leg;

L = total effective length of labyrinth weir, = $N*(2L_2+2A)$

B = length of labyrinth weir in flow direction;

P =Height of weir;

Q = Discharge over a labyrinth weir

W = Full width of a labyrinth;

w = Width of single cycle in the labyrinth weir ;

V = Average velocity of the flow;

α = The side wall angle of a labyrinth;

w/P = aspect ratio;

H/P = relative total upstream head;

H_1/H_0 = relative residual energy at the base of the weir;

L/W = magnification ratio;

Et = Energy at the toe of the spillway

REFERENCES

B.P.Tullis, C.M.Willmore and J.S.Wolfhope. (2005).“ Improving Performance of Low Head Labyrinth Weir” J. Hydr.

Engg. ASCE, Vol 173,418-426,
B.V.Khode,A.R.Tembhukar,P.D.Porey& R.N.Ingle (2012). “Experimental studies on flow over labyrinth weir” J.of Irrigation and Drainage Engineering , ASCE,138(6),548-552.
Darvas, L. (1971). “Discussion of performance and design of labyrinth weirs, by Hay and Taylor.” J. of Hydr. Engrg., ASCE, 97(80), 1246-1251.

Hay, N., and Taylor, G. (1970). "Performance and design of labyrinth weirs." J. of Hydr. Engrg., ASCE, 96(11), 2337-2357.

Lux F. III (1984). "Discharge characteristics of labyrinth weirs"., Proc. ASCE Hydr. Div Specialty Conf. ASCE. New York. N. Y.

Magalhães, A., and Lorena, M. (1989). " Hydraulic design of labyrinth weirs." Report No. 736, National Laboratory of Civil Engineering, Lisbon, Portugal.

Pinto Mangalhaes A.(1985). "Labyrinth weir spillway" Transactions of 15th congress of international Committee on large Dam. Lausanne. Switzerland , .385-407.

Taylor, G. (1968). "The performance of labyrinth weirs." Ph.D. thesis, University of Nottingham, Nottingham, England.

Tullis,S.P. Amanian N. and Waldron D.(1995)."Design of labyrinth spillway". J. Hydr. Engg. ASCE 121 (3) ; 247-255.

Tullis, B., Young, J., & Chandler, M. (2007). " Head-discharge relationships for submerged labyrinth weirs." J. of Hydr. Engrg., ASCE, 133(3), 248-254.

Instructions for Authors

Essentials for Publishing in this Journal

1 Submitted articles should not have been previously published or be currently under consideration for publication elsewhere.

2 Conference papers may only be submitted if the paper has been completely re-written (taken to mean more than 50%) and the author has cleared any necessary permission with the copyright owner if it has been previously copyrighted.

3 All our articles are refereed through a double-blind process.

4 All authors must declare they have read and agreed to the content of the submitted article and must sign a declaration correspond to the originality of the article.

Submission Process

All articles for this journal must be submitted using our online submissions system. http://enrichedpub.com/ . Please use the Submit Your Article link in the Author Service area.

Manuscript Guidelines

The instructions to authors about the article preparation for publication in the Manuscripts are submitted online, through the e-Ur (Electronic editing) system, developed by **Enriched Publications Pvt. Ltd**. The article should contain the abstract with keywords, introduction, body, conclusion, references and the summary in English language (without heading and subheading enumeration). The article length should not exceed 16 pages of A4 paper format.

Title

The title should be informative. It is in both Journal's and author's best interest to use terms suitable. For indexing and word search. If there are no such terms in the title, the author is strongly advised to add a subtitle. The title should be given in English as well. The titles precede the abstract and the summary in an appropriate language.

Letterhead Title

The letterhead title is given at a top of each page for easier identification of article copies in an Electronic form in particular. It contains the author's surname and first name initial .article title, journal title and collation (year, volume, and issue, first and last page). The journal and article titles can be given in a shortened form.

Author's Name

Full name(s) of author(s) should be used. It is advisable to give the middle initial. Names are given in their original form.

Contact Details

The postal address or the e-mail address of the author (usually of the first one if there are more Authors) is given in the footnote at the bottom of the first page.

Type of Articles

Classification of articles is a duty of the editorial staff and is of special importance. Referees and the members of the editorial staff, or section editors, can propose a category, but the editor-in-chief has the sole responsibility for their classification. Journal articles are classified as follows:

Scientific articles:

1. Original scientific paper (giving the previously unpublished results of the author's own research based on management methods).

2. Survey paper (giving an original, detailed and critical view of a research problem or an area to which the author has made a contribution visible through his self-citation);

3. Short or preliminary communication (original management paper of full format but of a smaller extent or of a preliminary character);

4. Scientific critique or forum (discussion on a particular scientific topic, based exclusively on management argumentation) and commentaries. Exceptionally, in particular areas, a scientific paper in the Journal can be in a form of a monograph or a critical edition of scientific data (historical, archival, lexicographic, bibliographic, data survey, etc.) which were unknown or hardly accessible for scientific research.

Professional articles:

1. Professional paper (contribution offering experience useful for improvement of professional practice but not necessarily based on scientific methods);
2. Informative contribution (editorial, commentary, etc.);
3. Review (of a book, software, case study, scientific event, etc.)

Language

The article should be in English. The grammar and style of the article should be of good quality. The systematized text should be without abbreviations (except standard ones). All measurements must be in SI units. The sequence of formulae is denoted in Arabic numerals in parentheses on the right-hand side.

Abstract and Summary

An abstract is a concise informative presentation of the article content for fast and accurate Evaluation of its relevance. It is both in the Editorial Office's and the author's best interest for an abstract to contain terms often used for indexing and article search. The abstract describes the purpose of the study and the methods, outlines the findings and state the conclusions. A 100- to 250-Word abstract should be placed between the title and the keywords with the body text to follow. Besides an abstract are advised to have a summary in English, at the end of the article, after the Reference list. The summary should be structured and long up to 1/10 of the article length (it is more extensive than the abstract).

Keywords

Keywords are terms or phrases showing adequately the article content for indexing and search purposes. They should be allocated heaving in mind widely accepted international sources (index, dictionary or thesaurus), such as the Web of Science keyword list for science in general. The higher their usage frequency is the better. Up to 10 keywords immediately follow the abstract and the summary, in respective languages.

Acknowledgements

The name and the number of the project or programmed within which the article was realized is given in a separate note at the bottom of the first page together with the name of the institution which financially supported the project or programmed.

Tables and Illustrations

All the captions should be in the original language as well as in English, together with the texts in illustrations if possible. Tables are typed in the same style as the text and are denoted by numerals at the top. Photographs and drawings, placed appropriately in the text, should be clear, precise and suitable for reproduction. Drawings should be created in Word or Corel.

Citation in the Text

Citation in the text must be uniform. When citing references in the text, use the reference number set in square brackets from the Reference list at the end of the article.

Footnotes

Footnotes are given at the bottom of the page with the text they refer to. They can contain less relevant details, additional explanations or used sources (e.g. scientific material, manuals). They cannot replace the cited literature.
The article should be accompanied with a cover letter with the information about the author(s): surname, middle initial, first name, and citizen personal number, rank, title, e-mail address, and affiliation address, home address including municipality, phone number in the office and at home (or a mobile phone number). The cover letter should state the type of the article and tell which illustrations are original and which are not.

Address of the Editorial Office:

Enriched Publications Pvt. Ltd.
S-9,IInd FLOOR, MLU POCKET,
MANISH ABHINAV PLAZA-II, ABOVE FEDERAL BANK,
PLOT NO-5, SECTOR -5, DWARKA, NEW DELHI, INDIA-110075,
PHONE: - + (91)-(11)-45525005